

USAAMRDL-TR - 75-30

12
03



A MECHANISTIC MODEL FOR PREDICTION OF DUCTILE EROSION

AD A 0 1 3 8 3 3
North Carolina State University
Department of Materials Engineering
Raleigh, N.C. 27607

July 1975

Final Report for Period 1 January 1973 - 31 December 1974

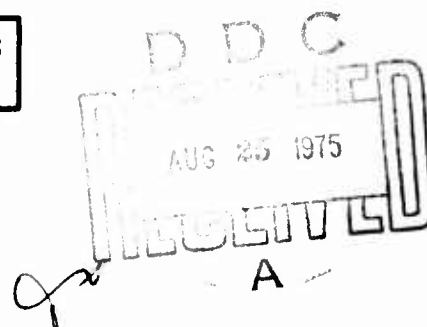
Approved for public release;
distribution unlimited.


Prepared for

EUSTIS DIRECTORATE

U. S. ARMY AIR MOBILITY RESEARCH AND DEVELOPMENT LABORATORY

Fort Eustis, Va. 23604



ACCESSION FOR	
NTIS	Write Section <input checked="" type="checkbox"/>
DOC	Read Section <input type="checkbox"/>
UNANNOUNCED	<input type="checkbox"/>
JUSTIFICATION	
BY	
DISTRIBUTION/AVAILABILITY CODES	
Dist.	Av.
	

EUSTIS DIRECTORATE POSITION STATEMENT

The work reported herein represents a new approach to mathematical modeling of the erosion process. The model developed uses the thermodynamic properties of the target material.

Although the data taken during the program indicated good correlation of the erosion rates predicted by the model with the erosion rates determined by test, further model verification will be required before the model is accepted. If the model is verified, it will be a valuable gas turbine design tool.

Appropriate technical personnel of this Directorate have reviewed this report and concur with the conclusions contained herein.

David B. Cale of the Technology Applications Division served as Project Engineer for this effort.

DISCLAIMERS

The findings in this report are not to be construed as an official Department of the Army position unless so designated by other authorized documents.

When Government drawings, specifications, or other data are used for any purpose other than in connection with a definitely related Government procurement operation, the United States Government thereby incurs no responsibility nor any obligation whatsoever; and the fact that the Government may have formulated, furnished, or in any way supplied the said drawings, specifications, or other data is not to be regarded by implication or otherwise as in any manner licensing the holder or any other person or corporation, or conveying any rights or permission, to manufacture, use, or sell any patented invention that may in any way be related thereto.

Trade names cited in this report do not constitute an official endorsement or approval of the use of such commercial hardware or software.

DISPOSITION INSTRUCTIONS

Destroy this report when no longer needed. Do not return it to the originator.

Unclassified

SECURITY CLASSIFICATION OF THIS PAGE (When Data Entered)

REPORT DOCUMENTATION PAGE		READ INSTRUCTIONS BEFORE COMPLETING FORM
1. REPORT NUMBER USAAMRDL TR-75-30	2. GOVT ACCESSION NO.	3. RECIPIENT'S CATALOG NUMBER
4. TITLE (and Subtitle) A MECHANISTIC MODEL FOR PREDICTION OF DUCTILE EROSION.	5. TYPE OF REPORT & PERIOD COVERED Final Report, Covering Period 1 Jan 73 - 31 Dec 74.	6. PERFORMING ORG. REPORT NUMBER
7. AUTHOR(s) William H. Jennings, Charles R. Manning, Jr. William J. Head	8. CONTRACT OR GRANT NUMBER(s) DAAJ02-73-C-0028	
9. PERFORMING ORGANIZATION NAME AND ADDRESS North Carolina State University Department of Materials Engineering Raleigh, North Carolina 27607	10. PROGRAM ELEMENT, PROJECT, TASK AREA & WORK UNIT NUMBERS 62203A 1F162203A119 02 010 EK	
11. CONTROLLING OFFICE NAME AND ADDRESS U.S. Army Air Mobility Research and Development Laboratory, Eustis Directorate Ft. Eustis, Va. 23604	12. REPORT DATE July 1975	
14. MONITORING AGENCY NAME & ADDRESS (if different from Controlling Office)	13. NUMBER OF PAGES 67	
	15. SECURITY CLASS. (of this report) Unclassified	
	15a. DECLASSIFICATION/DOWNGRADING SCHEDULE	
16. DISTRIBUTION STATEMENT (of this Report) DA-1-F-162203-A-119 Approved for public release; distribution unlimited.		
17. DISTRIBUTION STATEMENT (of the abstract entered in Block 20, if different from Report) 1-F-162203-A-11902		
18. SUPPLEMENTARY NOTES		
19. KEY WORDS (Continue on reverse side if necessary and identify by block number) Ductile Erosion Turbine Erosion Erosion		
20. ABSTRACT (Continue on reverse side if necessary and identify by block number) Mechanisms operative in dust erosion of ductile materials were determined with the aid of scanning electron microscope studies. Dimensional analysis was employed in the development of a mathematical model for predicting erosion of ductile materials. The basis of the model was the predominant identified erosion mechanism, target melting. The model was verified in an erosion testing program. Target materials in the testing program were three stainless steels, two aluminum alloys, a beryllium-copper alloy, and a titanium alloy.		

DD FORM 1 JAN 73 1473A EDITION OF 1 NOV 65 IS OBSOLETE

Unclassified
SECURITY CLASSIFICATION OF THIS PAGE (When Data Entered)

408886

to
1473B
DN

from 1473A

Unclassified

SECURITY CLASSIFICATION OF THIS PAGE(When Data Entered)

Erosive agents were three dusts comprised of hard, angular particles and one dust with spherical particles. Maximum particle velocities were 130 or 250 meters per second.



1473B

Unclassified

SECURITY CLASSIFICATION OF THIS PAGE(When Data Entered)

TABLE OF CONTENTS

	<u>Page</u>
LIST OF ILLUSTRATIONS	4
LIST OF TABLES	6
INTRODUCTION	7
LITERATURE SURVEY	8
APPROACH TO PROBLEM	11
APPARATUS	12
PROCEDURE	18
RESULTS AND DISCUSSION	20
DEVELOPMENT AND VERIFICATION OF THERMODYNAMIC EROSION MODEL	58
CONCLUSIONS	66
REFERENCES	67

LIST OF ILLUSTRATIONS

<u>Figure</u>		<u>Page</u>
1	Schematic Diagram of Erosion Test Facility	14
2	Impingement Angle Convention	15
3	Measurements Needed for Particle Roundness	15
4	Pitot Tube in Lathe Crosshead	17
5	Doubly Exposed Photograph of Particles Impinging on a Test Specimen	19
6	Maximum Airstream Velocity as a Function of Pressure Drop	21
7	Velocity Profile of Erosion Test Facility	22
8	Low Velocity Erosion of 17-7PH Stainless	24
9	Low Velocity Erosion of 17-4PH Stainless	25
10	Low Velocity Erosion of 302 Stainless	26
11	Low Velocity Erosion of 355 Aluminum	27
12	Low Velocity Erosion of 7178 Aluminum	28
13	Low Velocity Erosion of BC 25	29
14	Low Velocity Erosion of Ti 6Al-4V	30
15	High Velocity Erosion of 17-7PH Stainless	32
16	High Velocity Erosion of 17-4PH Stainless	33
17	High Velocity Erosion of 302 Stainless	34
18	High Velocity Erosion of 355 Aluminum	35
19	High Velocity Erosion of 7178 Aluminum	36
20	High Velocity Erosion of BC 25	37
21	High Velocity Erosion of Ti 6Al-4V	38

<u>Figure</u>		<u>Page</u>
22	Severely Deformed Aluminum Surface	39
23	Plastic Deformation of an Eroded Surface	40
24	1100 Aluminum Eroded by SiC	41
25	Deformed Surface of Titanium Alloy	42
26	Impact Craters in 302 Stainless	43
27	Melted Area on Titanium 6-4	45
28	Molten Droplet in the Bottom of an Impact Crater	46
29	Minute Erosion Debris	47
30	Possible Splattered Droplets	48
31	Particle Deposition Craters in Aluminum Surface	49
32	Surface of Aluminum Eroded by SiC	50
33	Ridges Pushed Up by Impacting Silicon Carbide Particles	51
34	Ridges Produced by Impacting Glass Beads	52
35	Well-Defined Ridge from a Single Glass Bead	53
36	Silicon Carbide Impacting Titanium at 30°	54
37	Ridge that is Flaking Off after Further Impacts	55
38	Severely Worked Ridges on 355 Aluminum	56
39	Ridges That Are About To Be Detached	57
40	Line Fit of Erosion vs $Z_{\text{Transferred}}$	63
41	Erosion vs Z_{Impact}	65

LIST OF TABLES

<u>Table</u>		<u>Page</u>
1	Typical Mechanical Properties of Target Materials	12
2	Roundness Factor for Particles	20
3	Impact and Rebound Velocities	23
4	Units of Model Terms	59
5	Selected Thermal Properties of Target Materials	60
6	Conversion Units	60
7	Combinations of Variables Employed in Erosion Model Verification	61

INTRODUCTION

Erosion of components by impacting dust particles is a serious problem for designers, manufacturers, and operators of mechanical systems. Erosion is particularly acute when turbine machinery is operated in dusty environments; an example is the well-documented experience of United States military forces and their operations of helicopters in Southeast Asia.¹

Filtration of intake air has alleviated the engine erosion problem somewhat. In helicopter operations, however, filtration reduces both payload and engine performance. A more desirable alternative is the production of an erosion-resistant or at least erosion-tolerant engine. This alternative requires that erosion be a basic design consideration.

Two items are needed before erosion can be treated objectively in the design process: an understanding of the basic operative mechanisms of erosion and a technique for predicting the amount or rate of erosion which will occur under given conditions. Consequently, the objectives of this study are twofold: to achieve an understanding of the means or mechanisms by which erosion occurs, and to develop a readily usable predictive model of erosion based on the identified mechanisms.

LITERATURE SURVEY

In the early work of Finnie,² it was contended that the major material removal mechanism in erosion was a mechanical process termed cutting wear or micromachining. Finnie wrote the equations of motion of a rigid particle impacting the surface of an annealed steel target. He found that important variables in the erosion process were: the mass and velocity of the eroding particles as well as their shape, hardness, and strength; the assumed constant plastic flow stress of the target material; and the apparent impingement angle of the particles*.

The predictive model developed by Finnie indicated that no erosion would occur at normal impingement. This was contrary to experimental evidence, and empirical correction factors were proposed to improve the predictive ability of the model.

Bitter^{3,4} hypothesized that an additional mechanism was operative during erosion. He termed the mechanism deformation wear and indicated that erosion was the sum of two mechanical processes, cutting wear and deformation wear. Deformation wear occurred when the target surface was repeatedly deformed by impacting particles which caused the surface to work harden and crack. Propagation and spreading of the cracks resulted in material removal. Unfortunately, erosion tests must be performed in order to estimate certain parameters which appear in Bitter's predictive models. Consequently, his models cannot be used a priori to predict magnitude of erosion. However, one may use Bitter's relationships to assess the variation in erosion as a function of particle impingement angle. In addition, the relationships indicated that erosion occurred at and near normal impact due to material removal through deformation wear.

Neilson and Gilchrist⁵ simplified Bitter's relationships and re-emphasized the importance of deformation wear. The results of erosion tests are needed before one can determine a number of parameters which appear in the models developed by Neilson and Gilchrist. Again, a priori predictions of erosion are not feasible.

Tilly,⁶ in his work with nominally ductile targets, presented a concept of erosion which occurred in two stages. The primary stage was cutting wear. The second stage, or secondary erosion, occurred when erosive particles fragmented upon impact and were projected radially

*The apparent particle impingement angle is the angle which the stream in which the particles are entrained makes with the target, measured from the face of the target. The impingement angle is shown schematically in Figure 2.

from the impact site. Additional cutting wear was produced by the fragmented particles. Tilly found that secondary erosion was a minimum at low impingement angles and a maximum at normal impingement. He produced micrographs to support the secondary erosion concept. It was shown, however, that secondary erosion did not fully account for target volume loss at normal impingement.

Statistical techniques were used by Head and Harr⁷ in their development of predictive models of erosion. Although based on a large number of target material, particle, and system variables, their models for natural contaminants were limited in scope to impingement angles of less than approximately 75° and maximum particle impact velocities of approximately 185 meters per second.

Smeltzer et al.⁸ were the first investigators to propose predictive erosion models based on changes in the thermal regime of the target. Certain thermal phenomena, such as heating of the target during erosion, had been observed earlier by others.^{9,10} However, these phenomena were not investigated fully.

Smeltzer and his colleagues recognized that in a general deformation process, approximately 90 to 95% of the available external energy was dissipated in thermal modes (heating and melting) while the remaining energy produced mechanical work. They analyzed surfaces of a number of eroded targets by means of scanning electron microscopy and concluded that melting of the target was of major importance in the erosion process. In addition, they estimated that the available kinetic energy per impacting erosive particle was sufficiently great to melt the volume of target material removed per impacting particle. Two mechanisms of material removal were suggested in their work: melting of the surface beneath an impacting particle followed by splattering of the molten material, and bonding of solidified material to imbedded particles which in turn were removed by subsequent impacting particles. Models were developed on the basis of these mechanisms. The models were used to predict the erosive behavior of several metals. Reasonable agreement with observed behavior was achieved. The models were functions of parameters evaluated from the results of erosion tests; consequently, a priori predictions of erosion could not be made.

The findings of Smeltzer et al.,⁸ Wood,¹¹ and others support the contention that macro-mechanical properties of the target do not greatly influence erosion behavior when the material removal mechanisms are primarily thermal in nature. In their studies, variations in target ultimate tensile strength, yield strength, and hardness did not significantly affect erosion behavior. However, targets with differing thermal properties did exhibit significant differences in erosion behavior.

In summarizing recent reported work on erosion mechanisms, it appears that phenomena associated with target melting have received

increased attention. Investigators primarily concerned with erosion of metals have demonstrated considerable interest in predictive erosion models which were, at least in part, thermodynamically based. Presumably, this interest was stimulated by findings of heating and melting of nominally ductile materials subjected to erosive particles. Mechanisms operative in the erosion of nominally brittle materials and techniques for quantifying them remain obscure at this time.

Variables identified as having major effects on erosion were summarized in Reference 7. For convenience, a portion of that summary is reproduced below:

(1) "Impact regime variables. Primary among these are the apparent particle impingement angle, particle velocity and the distribution of velocities within an aggregation of particles. Probably also of some importance are the characteristics of the medium within which erosion takes place."

(2) "Target variables. These include the nature of the target as reflected in resistance to erosion Intuitively, target resistance should be a continuous function of other variables; for example, the apparent particle impingement angle."

(3) "Contaminant variables. These include particle size, shape and hardness. For heterogeneous erosive agents*, some assessment must also be made of the distribution of these variables."

Mechanisms of erosion have been proposed and variables identified. However, only one a priori predictive model of erosion has been developed.⁷ That model was statistically based; consequently, its utility is restricted to the ranges of variables employed in its development. All other predictive models of erosion contain parameters which must be evaluated from the results of erosion tests.

*Natural dusts are heterogeneous with respect to mineralogical composition.

APPROACH TO PROBLEM

A two-phase research program was devised to attain the project objectives. The phases were:

1. Determination and/or verification of the operative mechanisms of material removal during the erosion process.

2. Development of a predictive model of erosion for selected metallic targets which requires no a priori erosion testing for the determination of model parameters. The model should reflect actual erosion mechanisms identified or verified in the first phase. In addition, the model should reflect the effects of changes in target variables, impact regime variables, and contaminant (dust) variables.

A scanning electron microscope (SEM) was the major investigative tool used in the initial phase of the work reported here. Eroded target surfaces were examined and photographed in a scanning electron microscope. The photographs were first analyzed separately and then compared with similar photographs which had been obtained by other investigators. This procedure led to verification of the target melting phenomena reported by Smeltzer and his colleagues.⁸

In the second phase, an extensive testing program was completed in which seven metallic targets were eroded over a range of impingement angles by four test dusts. Specimens of all target material were eroded by specified quantities of each test dust at a constant, medium particle impact velocity. Impingement angle was varied in each test series. In addition, specimens of all target materials were eroded by all dusts at a higher particle impact velocity. Impingement angle was also varied in this series of tests. The observed or dependent variable in all of the erosion tests was target volume loss. Other parameters were also determined. These included particle impact and rebound velocities and particle roundness, a measure of particle shape.

Finally, the concepts of dimensional analysis were used in the development of a predictive erosion model. It was recognized that the physical significance of the model would be greatly enhanced if it were dimensionally homogeneous. A major component of dimensional analysis is a systematic technique for determining groupings of variables which are dimensionally homogeneous. Not only is homogeneity assured, but frequently considerable insight can be gained into the form of the relationships between variables. Major details of the dimensional analysis used in this study may be found in Reference 7.

APPARATUS

TARGET MATERIALS

Seven metals were used as target materials in this study. The metals were chosen to represent a range of properties and/or because they are currently in widespread use in turbine-machinery applications. The materials were:

1. 17-7PH TH 1050 steel (AMS 5528)
2. 17-4PH H 900 steel (AMS 5643)
3. 302 stainless steel, annealed (AMS 5055)
4. 355 T-6 aluminum (AMS 4212E)
5. 7178 T-6 aluminum (AMS 7178)
6. BC25 beryllium copper, 1/2 hard (AMS 4532B)
7. 6Al-4V titanium (AMS 4911)

The 17-7PH and 17-4PH steels were precipitation hardened alloys. The 302 stainless steel was in the annealed condition. Both of the aluminum specimens were in the T-6 tempered condition: 355 was a cast alloy, while 7178 was a wrought alloy. The beryllium copper material was also a precipitation hardened alloy, while the titanium was a solution treated and aged alloy. Representative mechanical properties of the materials are shown in Table 1.

TABLE 1.
TYPICAL MECHANICAL PROPERTIES OF TARGET MATERIALS

Target Material	Ultimate Tensile Stren. (10^4kg/cm^2)	Yield Stren. (10^4kg/cm^2)	Young's Modulus (10^6kg/cm^2)	Knoop Hardness No. (as received)
17-7PH	1.41	1.30	2.04	188
17-4PH	1.37	1.27	2.00	360
302 SS	0.633	0.281	1.97	180
355 Al	0.246	0.176	0.703	106
7178Al	0.619	0.548	0.731	221
BC 25	0.633	0.578	1.30	201
Ti6-4	0.949	0.920	1.16	334

All target test samples were approximately 2.5 cm wide, 5 cm long, and 0.3 cm thick except the 17-7PH and 17-4PH specimens which were approximately 0.2 cm and 0.13 cm thick, respectively.

TEST DUSTS

Four commercially available abrasive materials were used as the erosive agents or test dusts in this study. They were chosen on the basis of variations in properties. The four materials were:

1. Silicon carbide, -220 mesh
2. Zirconium oxide, -100 mesh
3. Glass beads, -200 mesh
4. AC coarse test dust ("Arizona road dust"), 0-200 μm

The silicon carbide was a very hard, angular material; the zirconium oxide was also angular but less hard than the silicon carbide. The glass beads were about as hard as silica, a major component of natural sands, but were round in shape. The AC coarse dust is heterogeneous, naturally occurring material which is used frequently as a standard dust in testing air cleaners and carburetors. The composition of AC coarse dust by weight is approximately 69% silica and 16% alumina, with the remainder being small amounts of other softer minerals.

EROSION DEVICE

The erosion device may be described as a precision sand-blast apparatus, consisting of four major parts (Figure 1). Shown in the figure are the hopper which contained the charge of erosive particles, a mixing chamber where the carrier gas and the particles were mixed, the acceleration tube (2.4 meters long, 0.635 cm inside diameter) which served to direct the dust-gas mixture onto the target, and the test chamber which contained the target specimen mounted in a holder. The holder was mounted on a shaft which permitted the apparent particle impingement angle to be varied by the operator from 0° to 90° . During a test, the impingement angle was held constant at a preselected value. In Figure 2 is shown the convention used in this study for measuring the apparent particle impingement angle.

PHOTOGRAPHIC EQUIPMENT

High speed photographic techniques were used in the determination of particle impact and rebound speeds. The equipment included a still camera, a dual flash light source, and a timer. The camera was a 9.2 x 12.7 cm format double bellows view camera equipped with a 210 mm focal length lens and a Polaroid film pack adaptor back. Polaroid black and white type 57 film was used in photographing the particles.

The light source was a dual flash device which employed a two-channel control unit and two xenon flash lamps. The time interval between flashes could be set at 1, 3, 10, 30, 100 or 300 μsec .

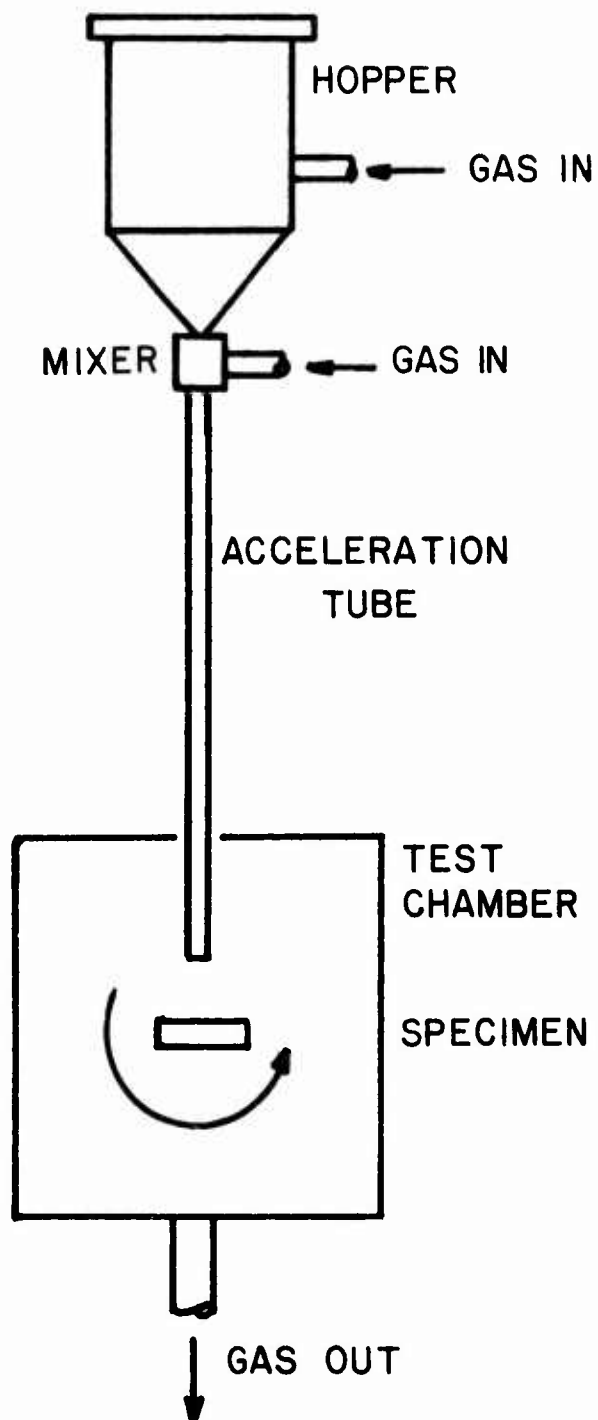


Figure 1. Schematic Diagram of Erosion Test Facility.

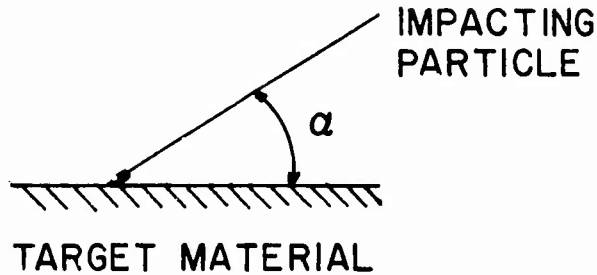


Figure 2. Impingement Angle Convention.

PARTICLE SHAPE ANALYZER

A Zeiss TGZ-3 particle analyzer was used to measure the shape factors of the test dusts. The instrument consists of a Plexiglas plate on which photographic negatives of the particles were placed and an adjustable iris diaphragm which was connected through a foot switch to a series of telephone counters. When the foot switch was depressed, a mark was entered on that counter corresponding to the diameter of the diaphragm. Simultaneously, a pointed marker descended and punched a small hole in the negative, thereby providing the operator with a visible record of the particles measured. The shape parameter used in this study was particle roundness employed by Head and Harr⁷ and defined as follows:

$$R = \Sigma c / I_R N \quad (1)$$

where R is the degree of roundness of a particle in one plane (dimensionless), c the radius of curvature of the individual corners, I_R the radius of the maximum inscribed circle, and N the number of corners measured. In Figure 3 are shown the measurements needed for determining particle roundness.

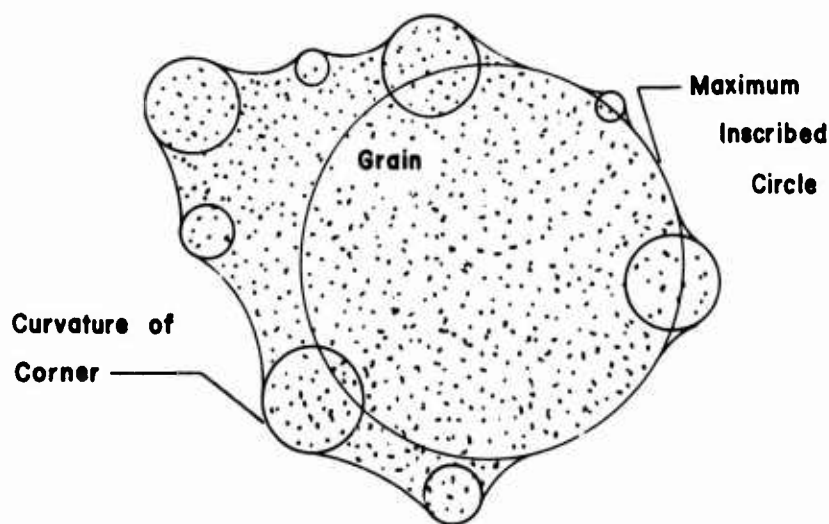


Figure 3. Measurements Needed for Particle Roundness.

Particle roundness is a measure of the "sharpness" or "angularity" of a particle. The greater the sharpness of the asperities of a particle, the smaller the value of roundness for that particle. The roundness value for a sphere is 1.0, while very sharp, angular particles have typical roundness values ranging from about 0.25 to 0.40.

TOTAL PRESSURE PROBE

A total pressure probe was employed in this study to determine both magnitude and distribution of the velocity of the gas emanating from the acceleration tube in the erosion device. The probe consisted of a Pitot tube connected to a mercury-filled U-tube manometer. The Pitot tube, mounted in a lathe crosshead to facilitate precise movement across the face of the acceleration tube, is shown in Figure 4. To obtain a gas stream velocity profile, the Pitot tube was aligned accurately with the acceleration tube, the carrier gas was admitted into the erosion device, and readings of the changes in mercury levels in the manometer were obtained as the Pitot tube traversed the gas stream. The collector of the Pitot tube was positioned 2.54 cm from the end of the acceleration tube, the same distance as a target in an erosion test. Differences in the heights of the mercury column were used in calculating the gas stream velocities.

SCANNING ELECTRON MICROSCOPE

A Jelco II scanning electron microscope was used in analyzing eroded target surfaces. The accelerating voltage was 25,000. Eroded surfaces of target materials noted previously were examined. In addition, specimens of eroded 1100 aluminum, both in the dead annealed and severely cold worked states, were examined. It was felt that the operative erosion mechanism might be more readily discernible with the 1100 aluminum samples than with specimens of the other target materials.

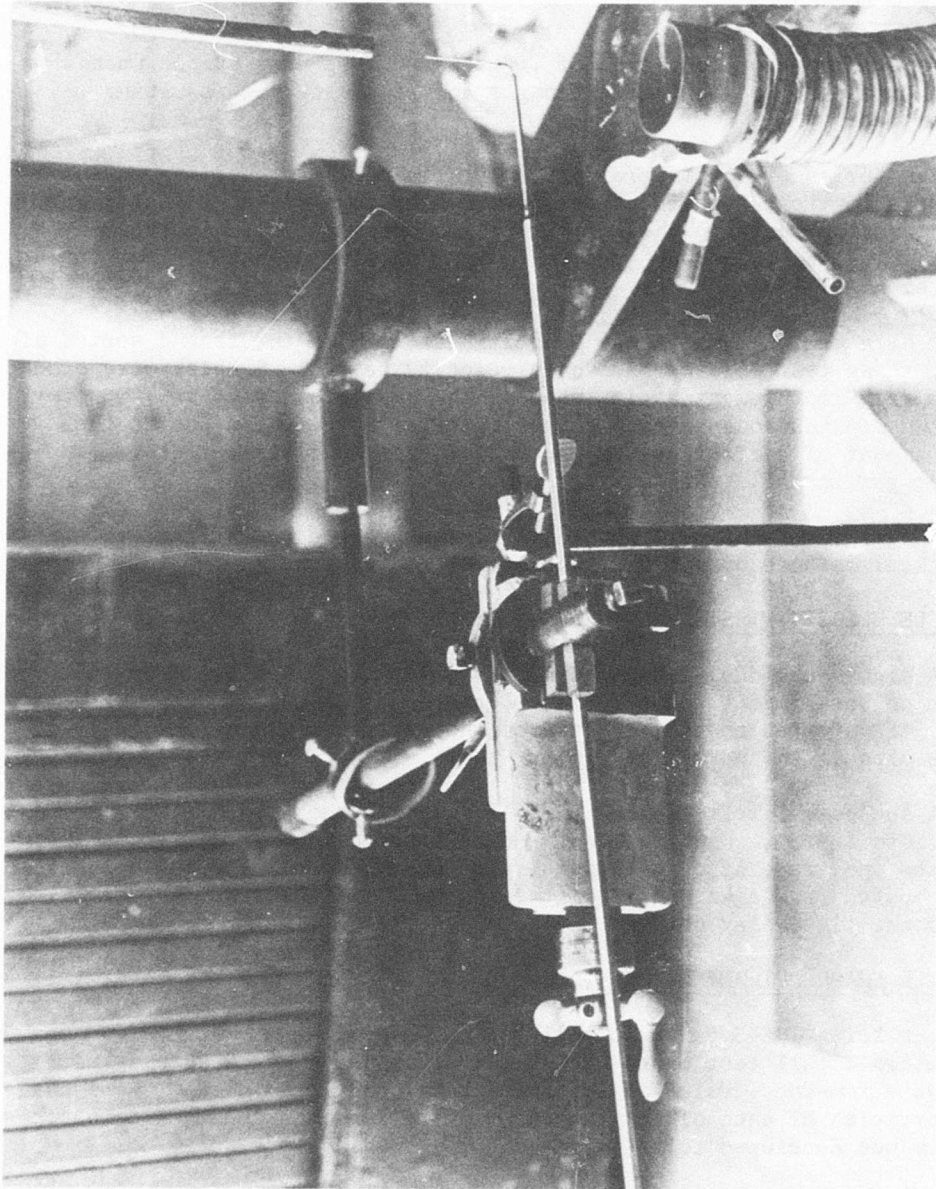


Figure 4. Pitot Tube in Lathe Crosshead.

PROCEDURE

EROSION TESTS

An erosion test consisted of impinging a 200g dust sample upon a target at a selected impingement angle and recording the resulting erosion rate*.

Two series of tests were performed. In the first series, termed "low velocity tests", a relatively low maximum gas stream velocity was used. Erosion tests in the series were conducted at five impingement angles: 20°, 30°, 45°, 60° and 90°. Four samples were tested at each impingement angle.

A high maximum gas stream velocity was used in the second series of tests; these test were termed "high velocity tests". Samples were eroded at the same impingement angles used in the low velocity tests. However, only two replications of each target material were eroded due to the large amount of carrier gas expended in the high velocity tests. The carrier gas for all tests was dry compressed air.

Target specimens were washed in acetone, dried and weighed on an analytical balance both before and after erosion testing.

PARTICLE VELOCITY TESTS

A high-speed dual-flash photographic technique was employed to determine both impact and rebound velocities of dust particles. Kinetic energy transferred to the target from the particles was estimated from the results of the particle velocity tests.

A successful test yielded a doubly exposed photograph (Figure 5) in which both impacting and rebounding particles could be seen. Each flash produced one image of an individual particle. The velocity of a particle was computed from a knowledge of the distance travelled by the particle during the time delay between flashes.

PARTICLE SHAPE DETERMINATIONS

The Zeiss TGZ-3 particle analyzer was used in determining the roundness parameters of all test dusts except the glass beads which were assumed to have a roundness value of 1.0 (perfectly spherical shape). More than 100 particles of each of the remaining dusts were analyzed. A computer program was developed to calculate the roundness values.

*Erosion rate was defined as the volume loss of the target per gram of dust impacted.

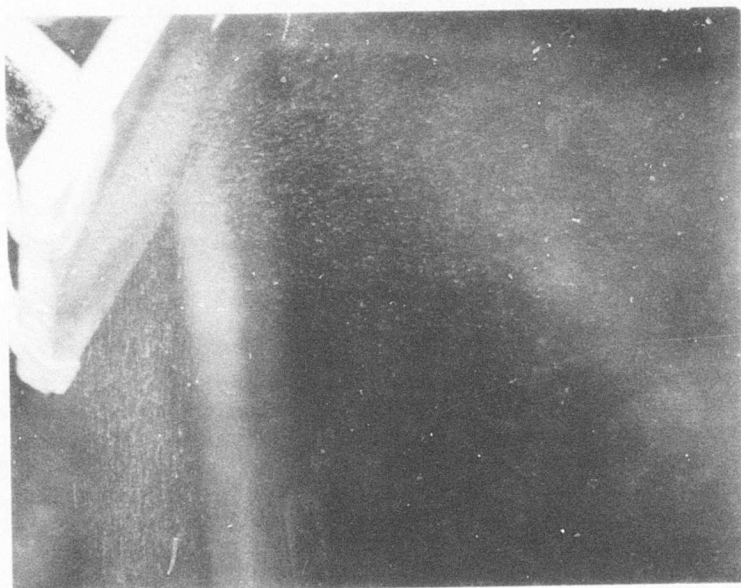


Figure 5. Doubly Exposed Photograph of Particles
Impinging on a Test Specimen.

RESULTS AND DISCUSSION

This section will cover results obtained from particle roundness testing (Table 2) and velocity determinations (Table 3 and Figures 6 and 7). Also covered will be erosion testing, Figures 8 through 21, and scanning electron microscopy, Figures 22 through 39.

PARTICLE ROUNDNESS

The various particles were analyzed for roundness as described in the procedure, and the results are shown in Table 2.

TABLE 2.
ROUNDNESS FACTOR FOR PARTICLES

<u>Particles</u>	<u>$R = \Sigma c/I_R N$</u>
Zirconia	0.316
AC Coarse	0.335
Silicon carbide	0.357
Glass beads	1.0

An examination of the values tabulated indicates that the particles are divided into two groups: the high R value shown by the glass beads which are known to be spherical, and the low values associated with the other three materials. The zirconia with the lowest value of R was the most angular, followed by the AC test dust and silicon carbide. The particle roundness factor will be correlated with the amount of erosion noted at various velocities.

VELOCITY DETERMINATION

Initially, the maximum air stream velocity obtainable vs pressure drop was investigated to set the velocity parameters. In Figure 6, maximum air stream velocity can be noted to peak at 189 m/sec using air pressures available. Using high pressure compressed air (1.69×10^8 dynes/cm²), velocities of 372 m/sec were obtained. Due to the construction of the equipment, a large number of runs at high compressed air pressures was not attempted. From the results above, the first velocity test of 189 m/sec was selected and high velocity test at 372 m/sec was selected.

The next important parameter was the velocity profile in the tube. This was determined using the Pitot tube and manometer; the results are

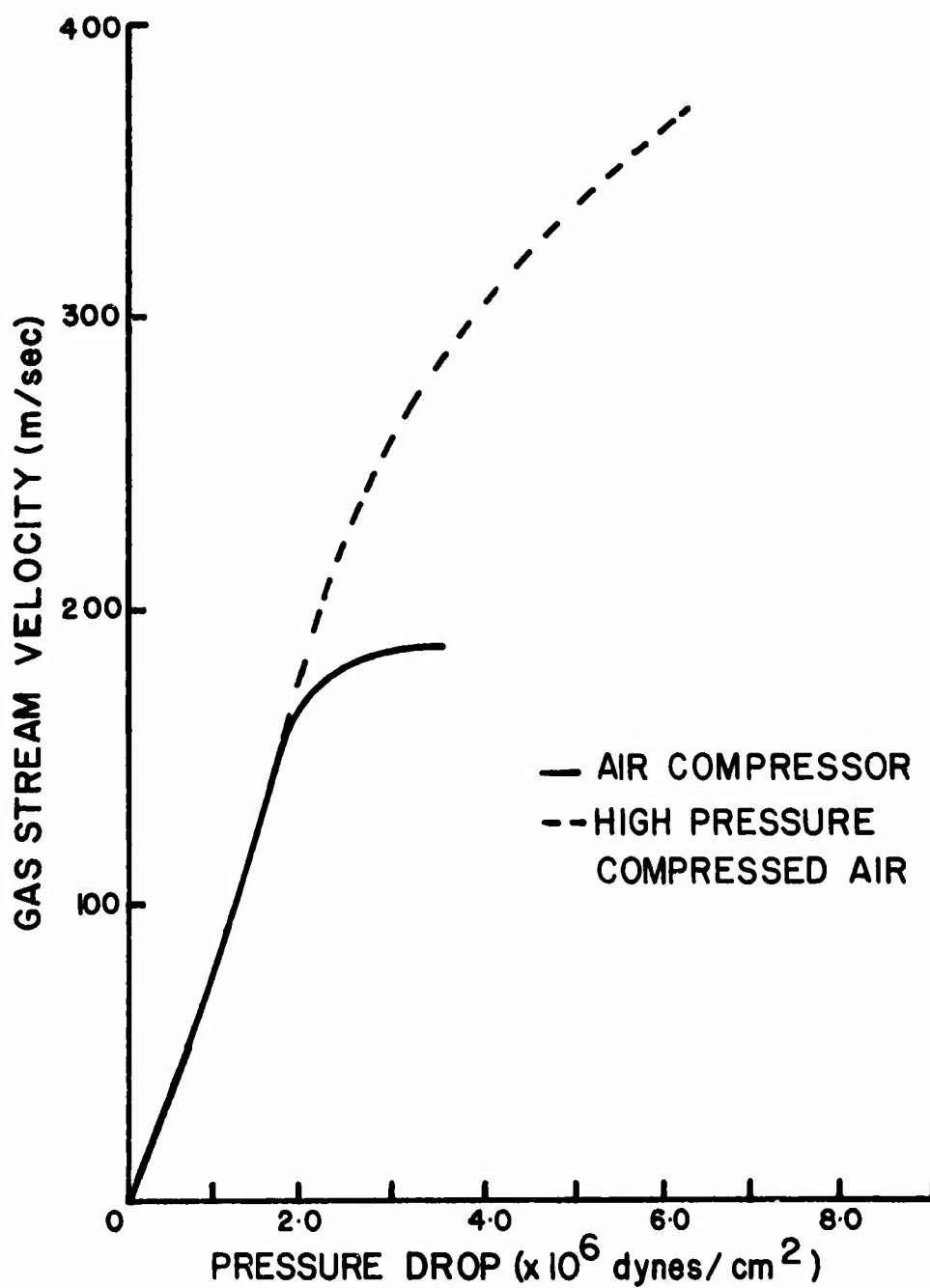


Figure 6. Maximum Airstream Velocity as a Function of Pressure Drop.

shown in Figure 7. The maximum velocity was noted at the center of the tube, and the velocity remains at 0.57 maximum velocity at a distance equal to the radius of the tube. The velocity profile noted above was obtained at a distance of 2.54 cm from the end of the tube. Accuracy of the air stream velocity measurements was within 1%.

In table 3, the results are tabulated for velocities at various impingement angles and particle roundness values for two alloys. There was a significant difference in particle impact velocity at the pressure drop of 2.20×10^6 dynes/cm² which represents the low velocity tests for the glass beads and the silicon carbide. The glass beads, with a high roundness number (1.0), impact at 91 m/sec while the low roundness sharp silicon carbide impacts at 145 m/sec. These results led to the expectation of a lower erosion rate for the glass beads than for the sharper particles. This was found to be the case and will be more obvious in

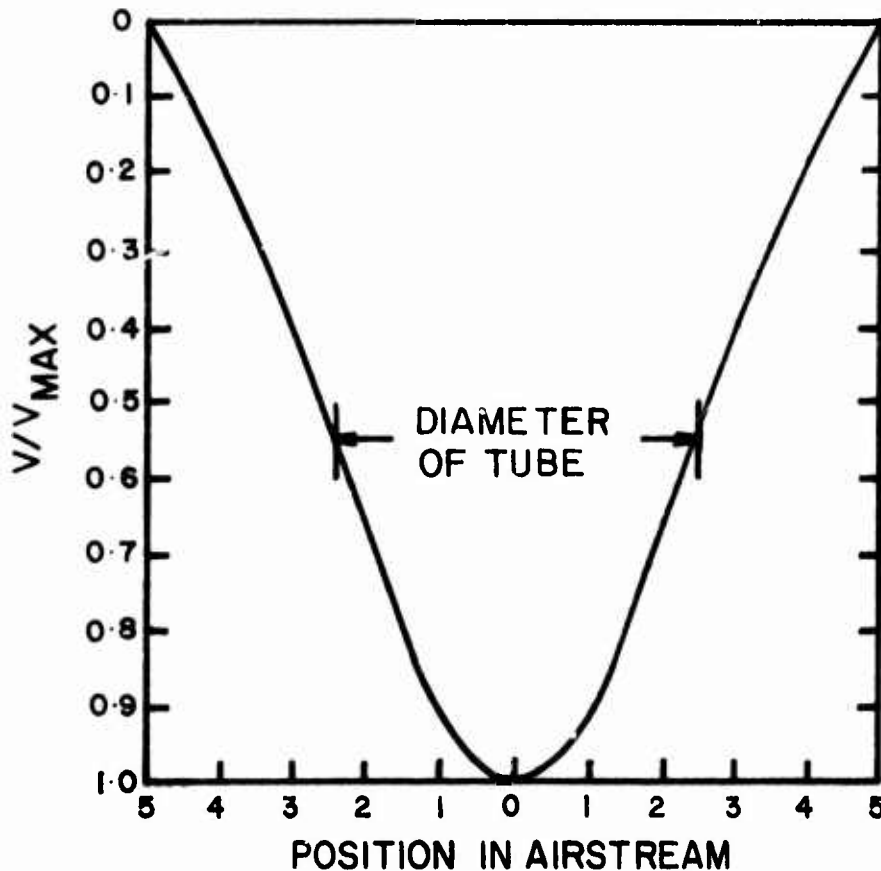


Figure 7. Velocity Profile of Erosion Test Facility.

the next section. For the higher pressure drop of 6.20×10^6 dynes/cm², which represents the high velocity tests, a very different behavior was noted. The impact velocities measured for glass beads and silicon carbide were 256 m/sec and 253 m/sec respectively, which represents a very small difference. This would lead one to the assumption that the erosion on a particular material would be similar. This was found to be fairly accurate.

TABLE 3.
IMPACT AND REBOUND VELOCITIES

<u>Material</u>	<u>Dust</u>	<u>α(deg.)</u>	<u>Pressure Drop</u>	<u>V_{Impact}</u> (m/sec)	<u>V_{Rebound}</u> (m/sec)
355 Al	GB	20	2.20×10^6 dynes/cm ²	91	35
		30			29
		45			52
		60			58
Ti 6-4	SiC	60	2.20×10^6 dynes/cm ²	145	58
355 Al	SiC	20	2.20×10^6 dynes/cm ²	145	34
		45			58
		60			58
Ti 6-4	GB	20	6.20×10^6 dynes/cm ²	256	87
		30			76
		45			73
Ti 6-4	SiC	20	6.20×10^6 dynes/cm ²	253	67
		30			91
		45			67

The third point to be made about the data was that rebound velocity varied with angle of impingement.

Test accuracy was ± 5 m/sec.

Tests on a strong, hard material (Ti 6-4) and a relatively soft, weak material (355 Al) were considered sufficiently representative. It was felt that the behavior of all the sharp, angular particles would be accurately reflected by the silicon carbide.

EROSION TESTS

The low-velocity erosion test results giving volume loss vs angle of impingement are shown in Figures 8-14. The volume loss normally reaches a maximum at some low angle, typically 20-30° for sharp, angular particles and 30-45° for glass beads. Erosion then decreases to a much lower value at normal impingement.

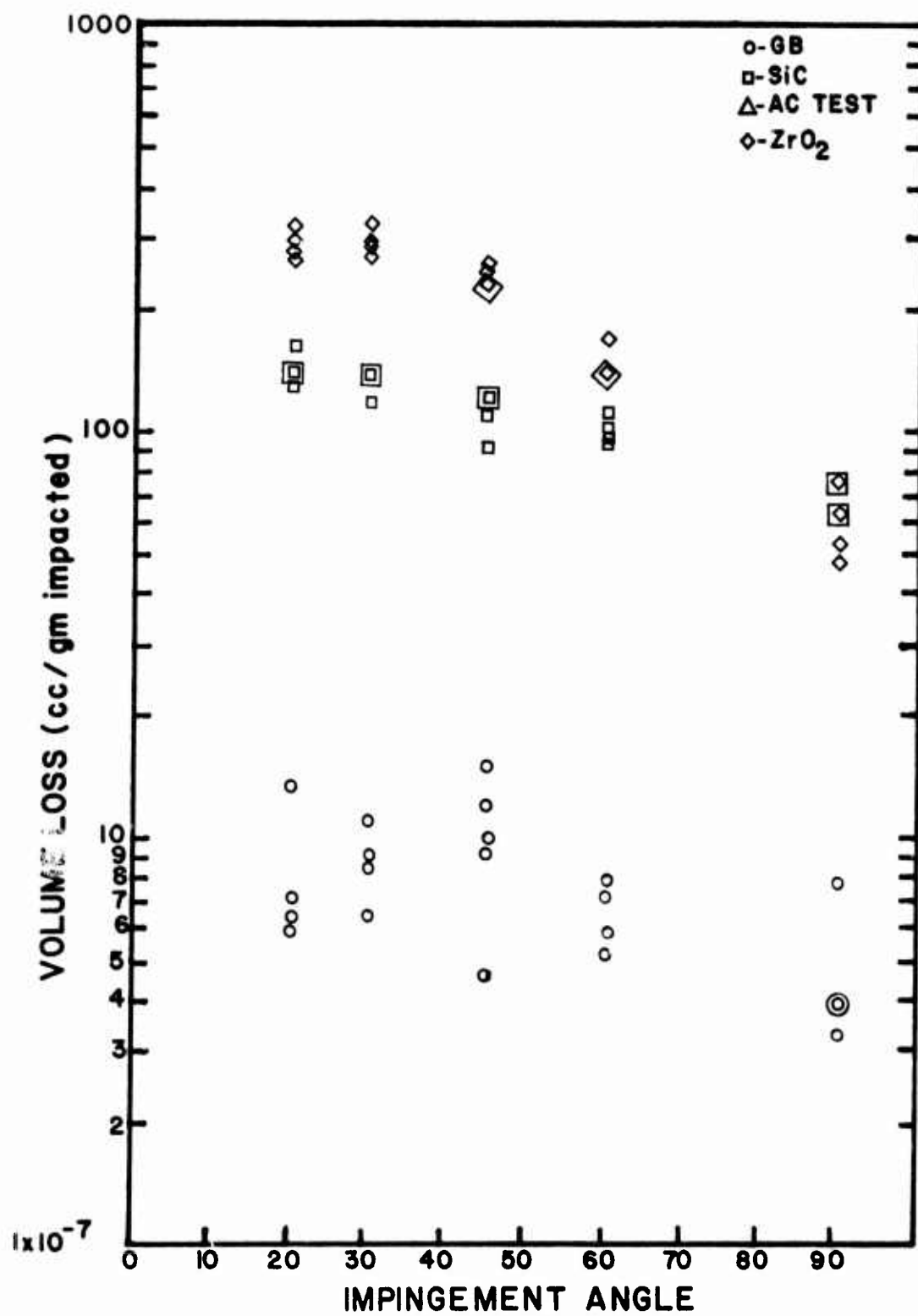


Figure 8. Low Velocity Erosion of 17-7PH Stainless.

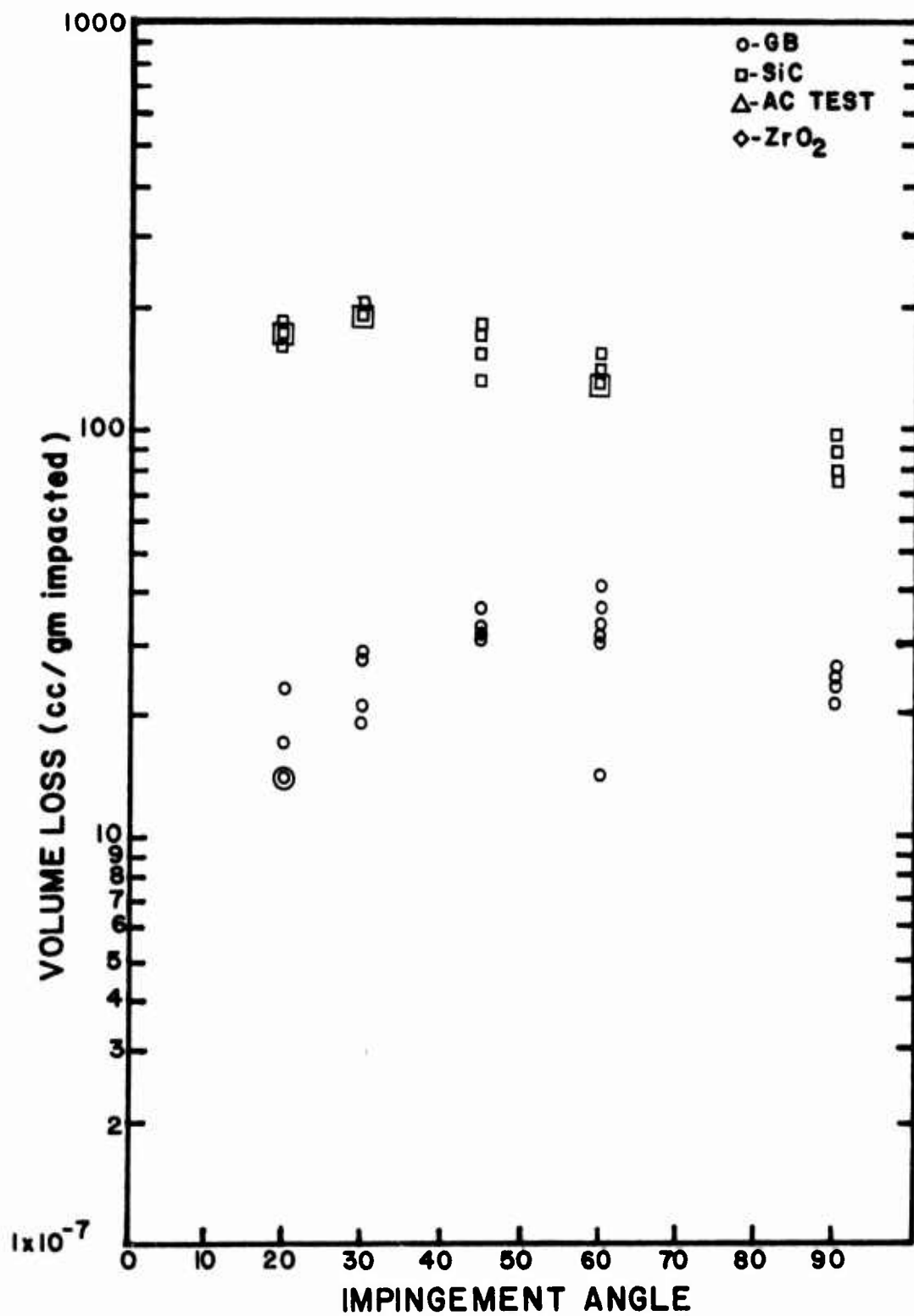


Figure 9. Low Velocity Erosion of 17-4PH Stainless.

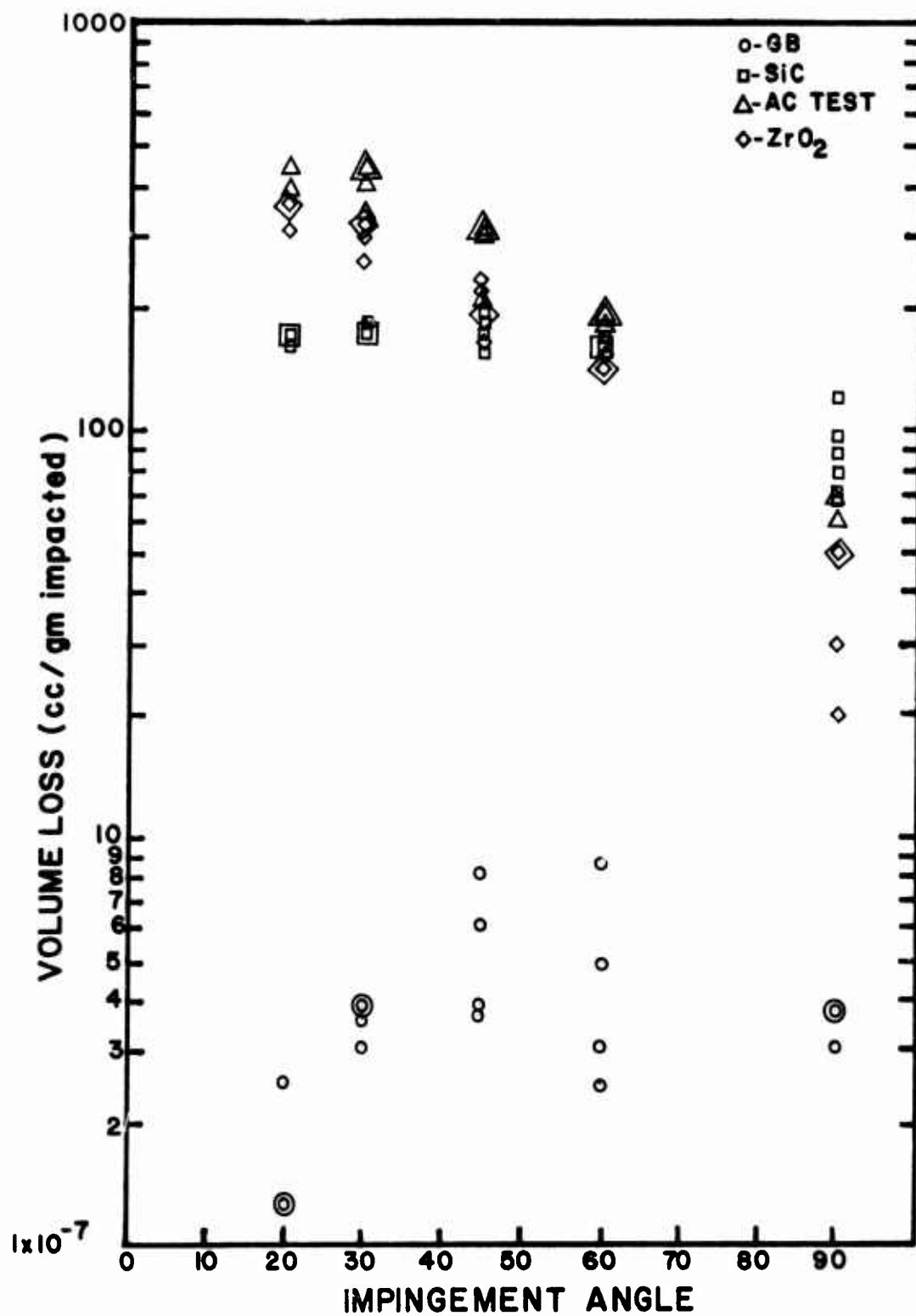


Figure 10. Low Velocity Erosion of 302 Stainless.

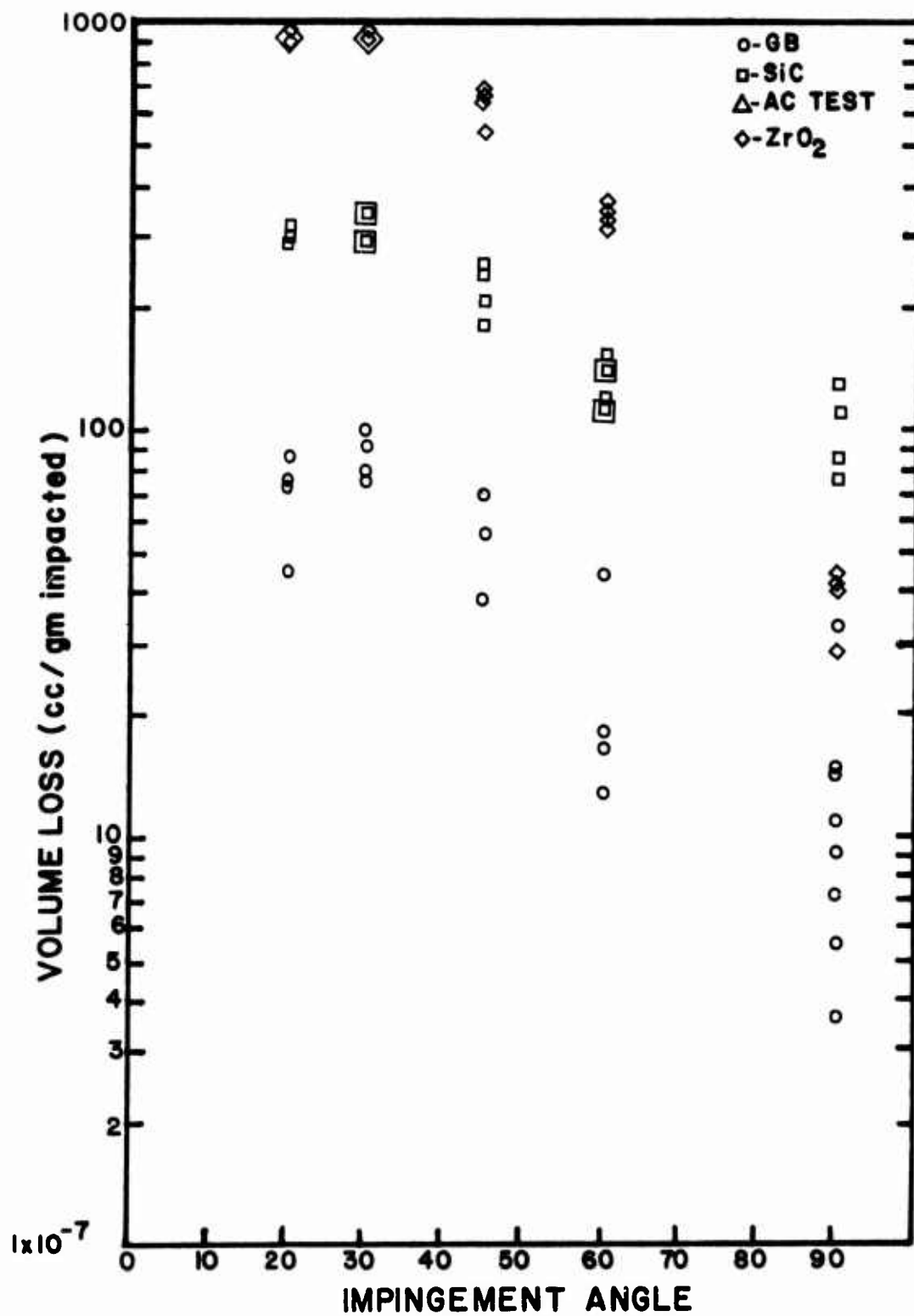


Figure 11. Low Velocity Erosion of 355 Aluminum.

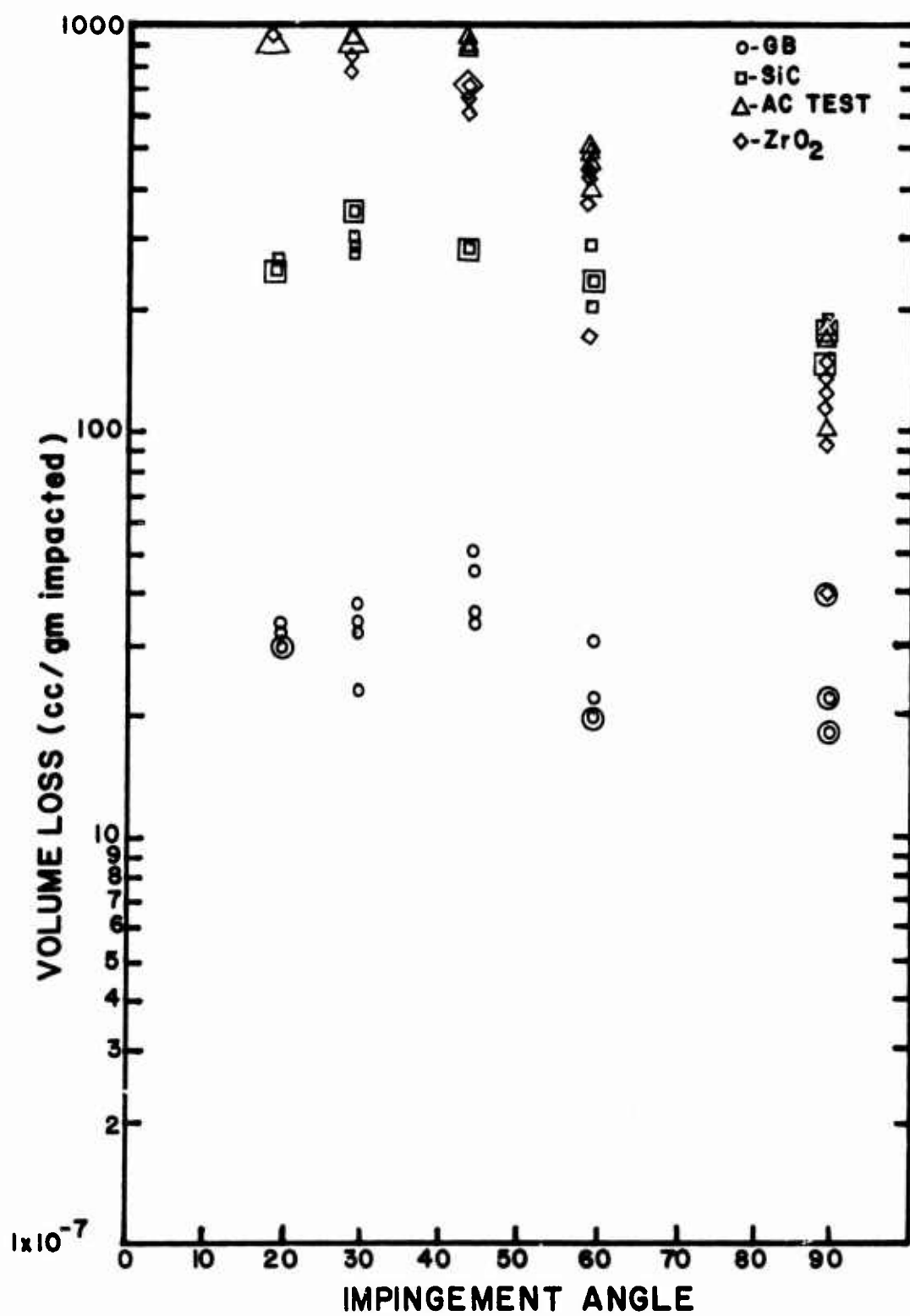


Figure 12. Low Velocity Erosion of 7178 Aluminum.

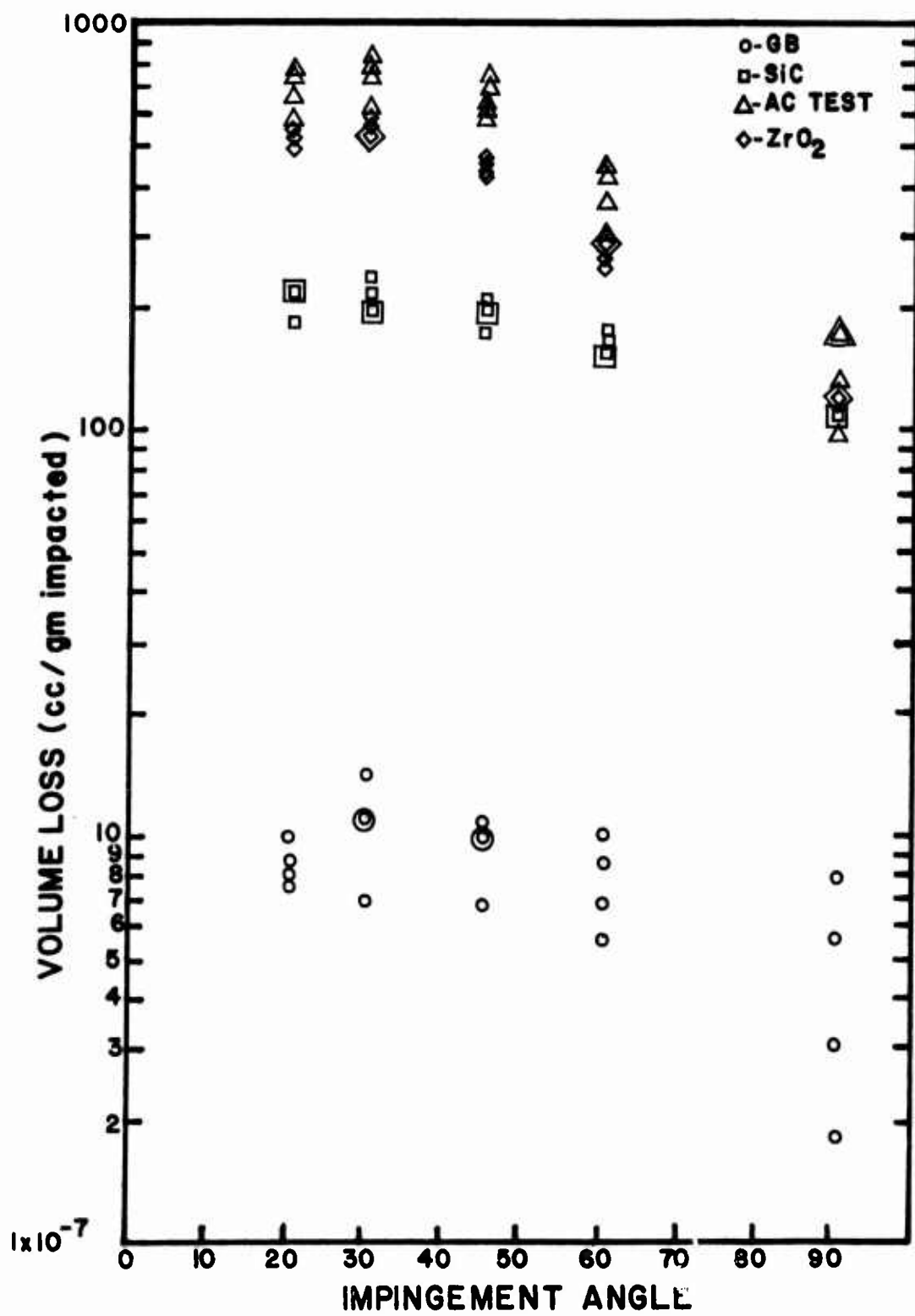


Figure 13. Low Velocity Erosion of BC 25.

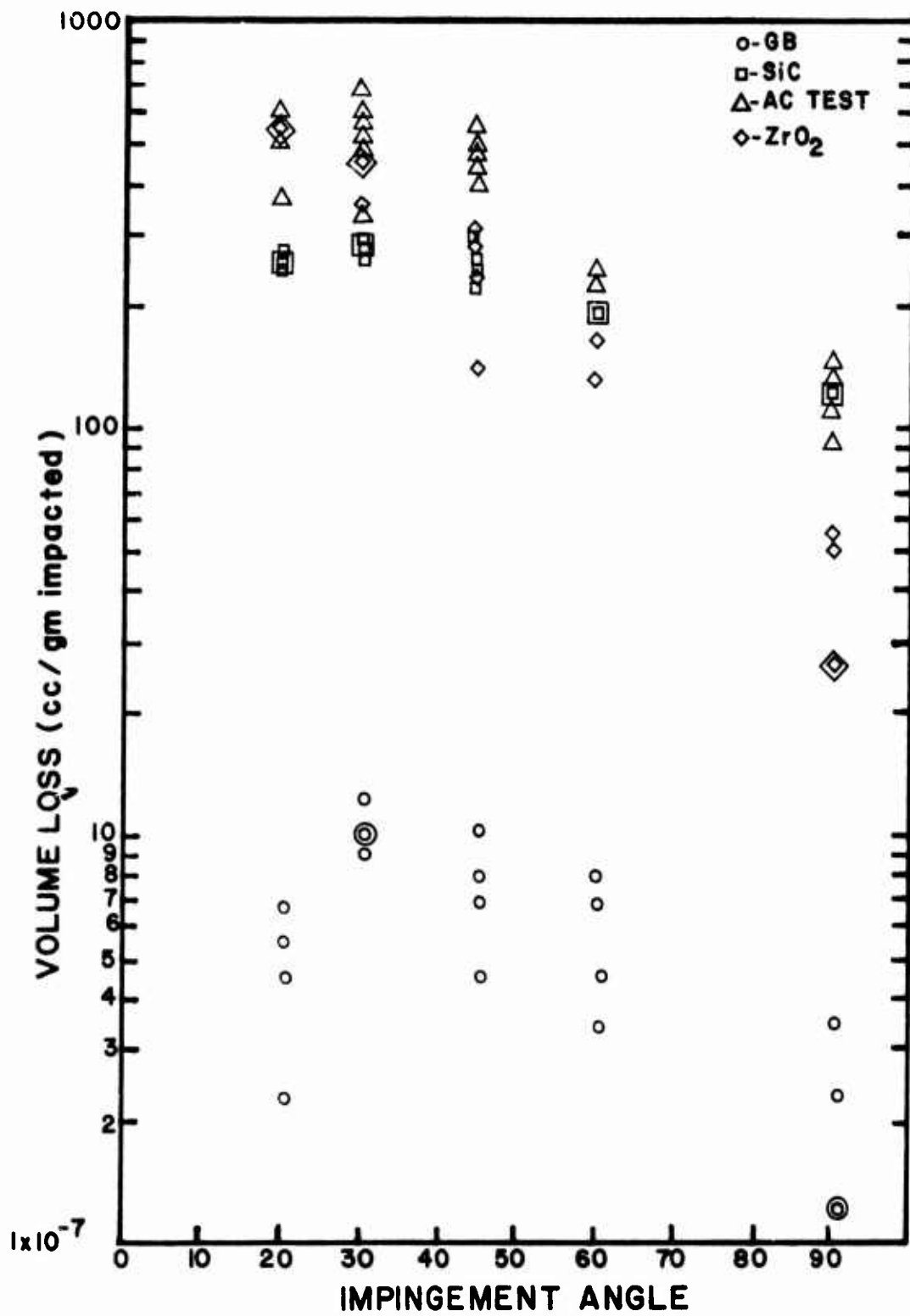


Figure 14. Low Velocity Erosion of Ti 6Al-4V.

In general, a great disparity was noted between the erosion produced by the sharp, angular particles and that produced by the glass beads. It varied from one to two orders of magnitude. This would be expected from the particle roundness and velocity results. Two exceptions to this were the aluminum alloys. The volume loss of eroded material noted for the two different types of particles was close for these two alloys. The amount of erosion for these two alloys was also higher, in general, than for the other materials.

The mechanical properties of the alloys could not be correlated with any trends in erosion behavior for all materials. One exception was that the two materials with the lowest elastic moduli (aluminum alloys 355 and 7178 with moduli approximately 0.55 that of the next lowest value) displayed the highest maximum erosion at this velocity and the minimum disparity between the glass beads and the sharp particles.

High-velocity test information is plotted in Figures 15-21. There was a marked decrease in the disparity between the amount of material eroded by the round and angular particles. The material eroded by low roundness number particles (angular particles) did not increase over the amount at low velocity for the most part. The amount of material eroded by the high roundness number particles did increase. At and near 90°, the values for eroded material for the round and angular were nearly the same, while at lower impingement angles, the sharp particles eroded more material. The exception was the aluminum, where there was essentially no difference.

These results seem to indicate that some energy input limit has been reached or exceeded for the operating material removal mechanism on the aluminum. After a certain energy level has been reached, the erosion process does not become more efficient. Other materials are close to reaching it also. These results support the melting theories of erosion. If melting was the primary erosion mechanism, then, after the minimum energy transfer needed for melting has been attained, added energy input would not influence the erosion rate to a great extent.

SCANNING ELECTRON MICROSCOPY

The general appearance of all samples examined under the scanning electron microscope was that of a severely deformed surface. Scanning electron micrographs of some surfaces are shown in Figures 22-25. From the large amount of plastic deformation of the surfaces, it appears that some type of heating effect occurred.

Several areas were found that appeared to be melted or where molten debris apparently had been deposited. A titanium sample (Figure 26) eroded at 45° with glass beads is indicative of an area that melted and

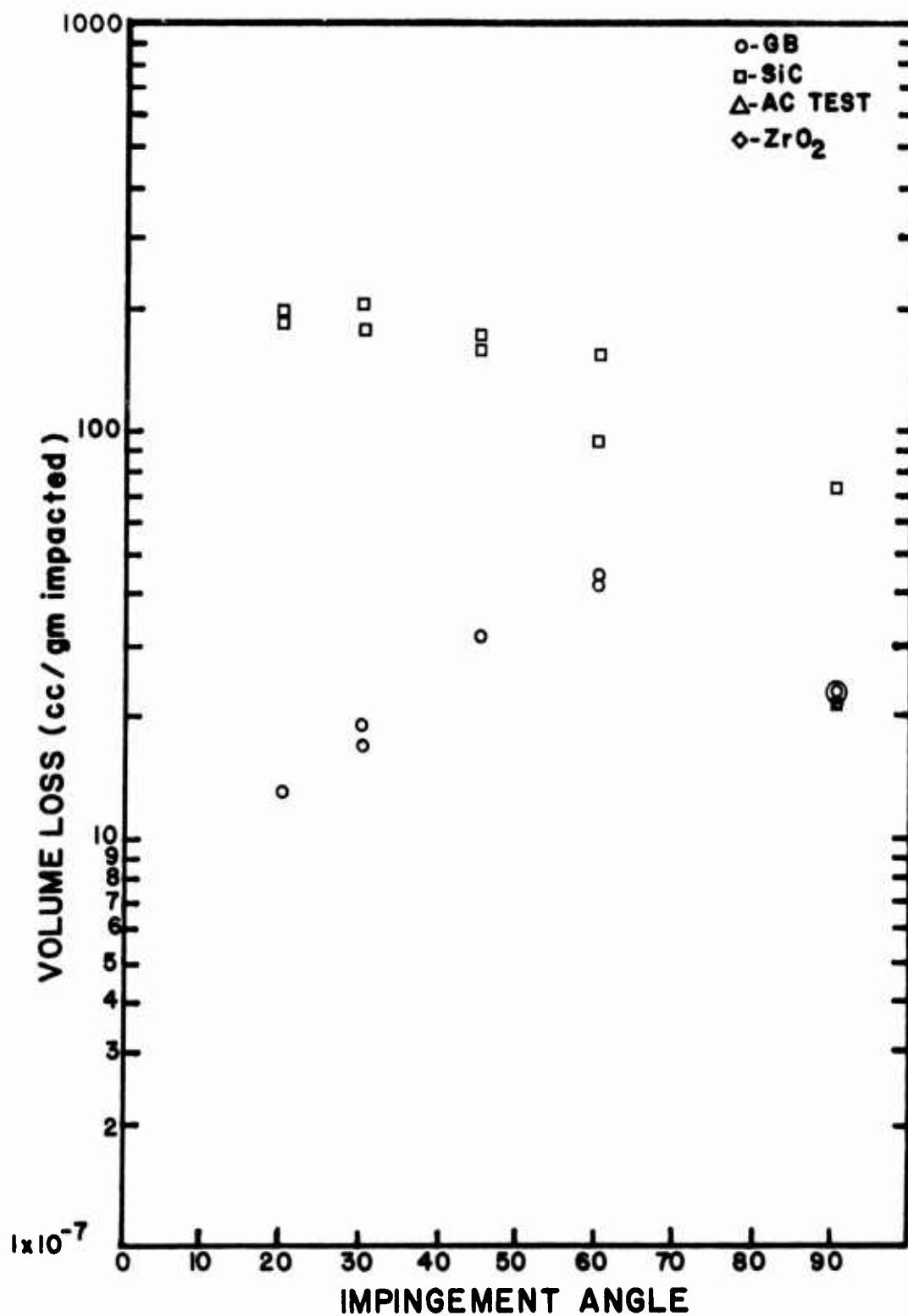


Figure 15. High Velocity Erosion of 17-7PH Stainless.

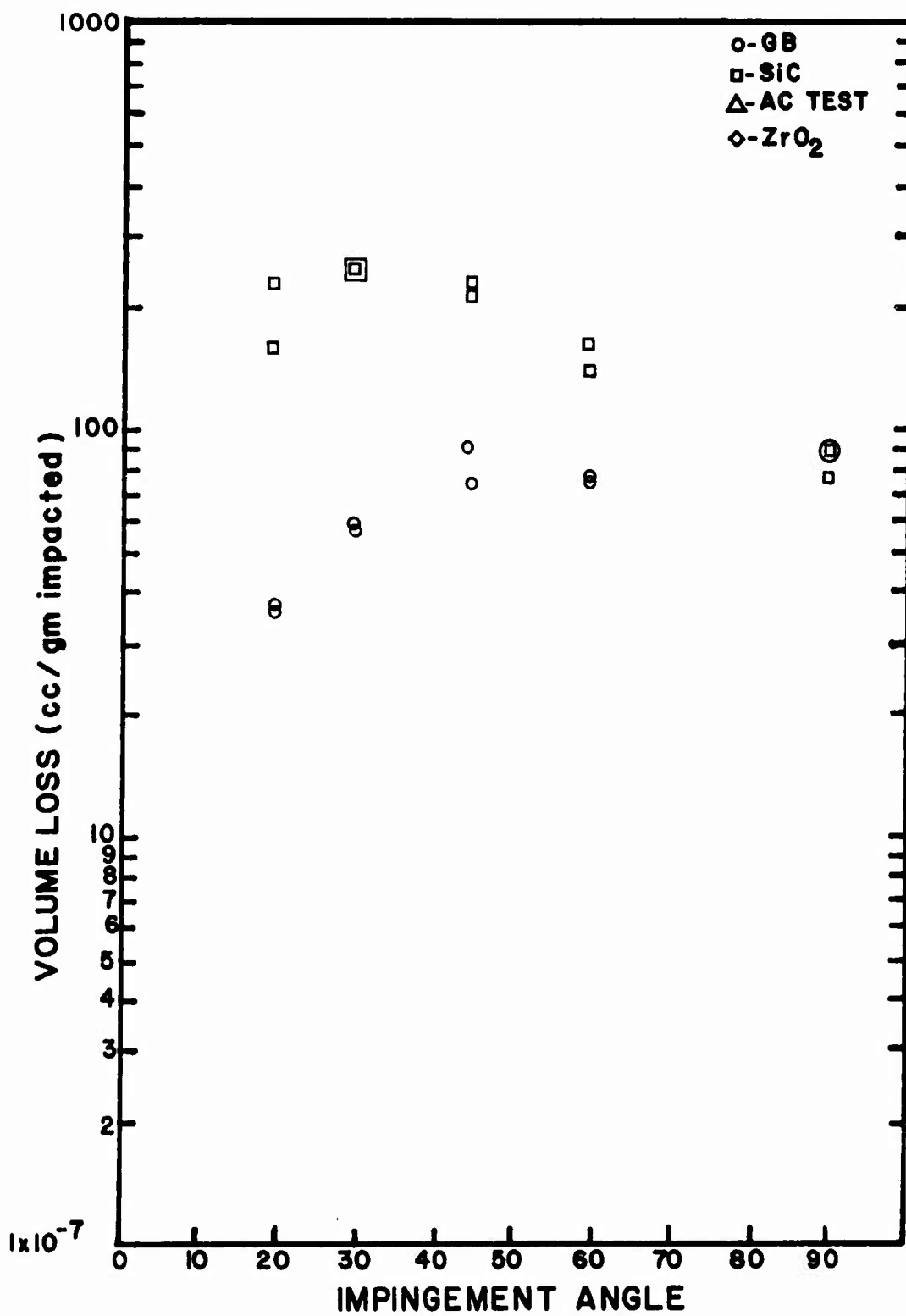


Figure 16. High Velocity Erosion of 17-4PH Stainless.

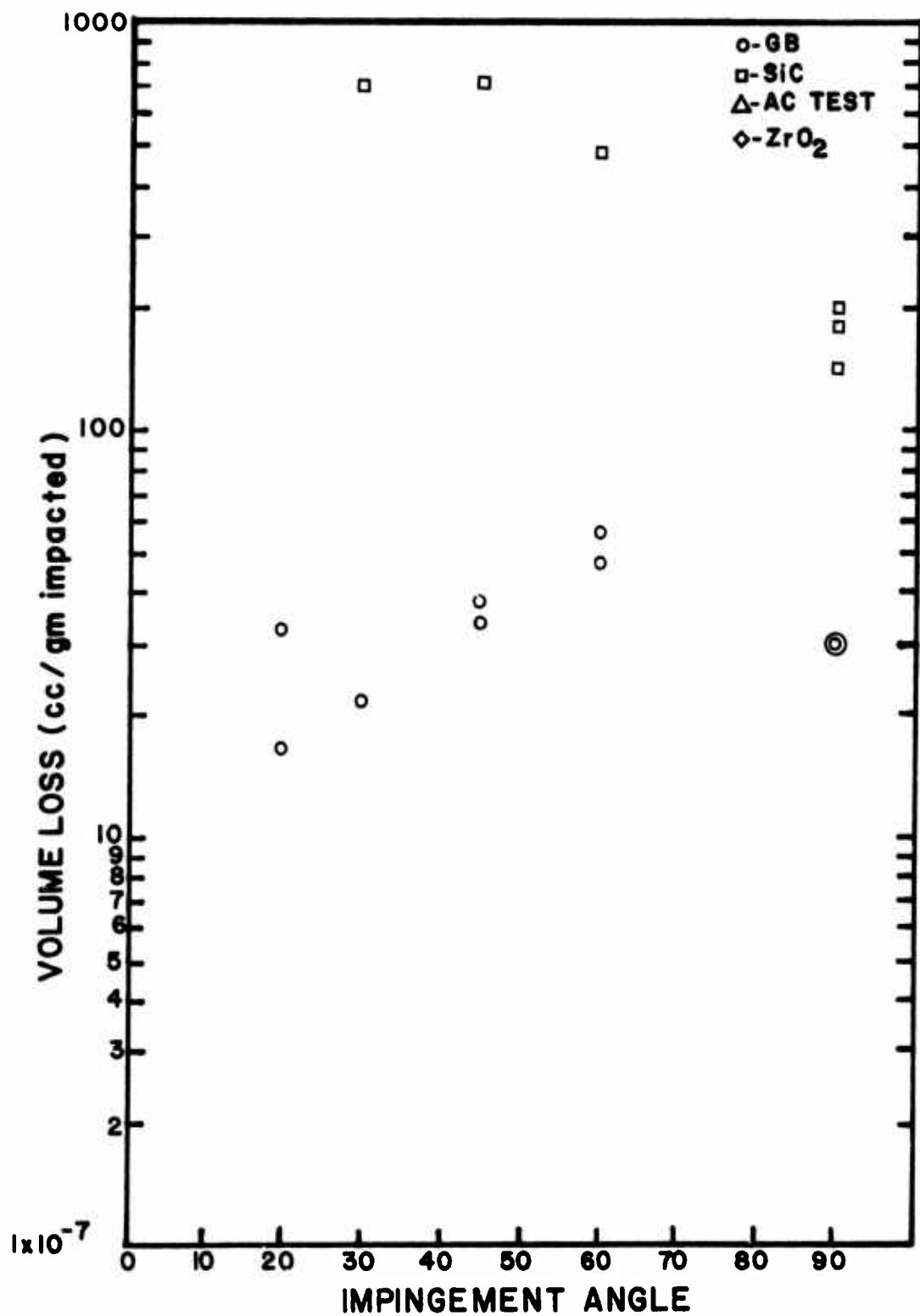


Figure 17. High Velocity Erosion of 302 Stainless.

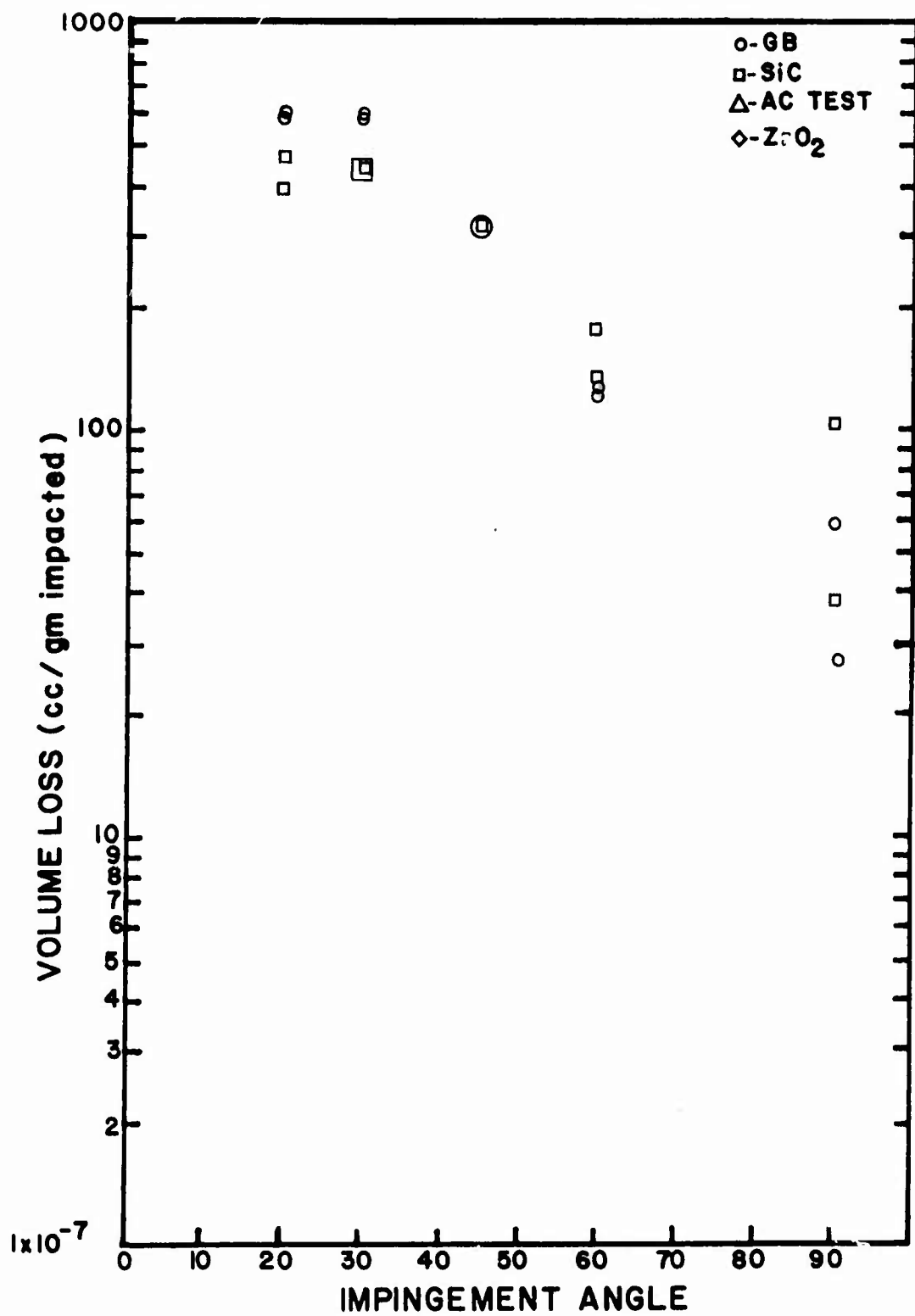


Figure 18. High Velocity Erosion of 355 Aluminum.

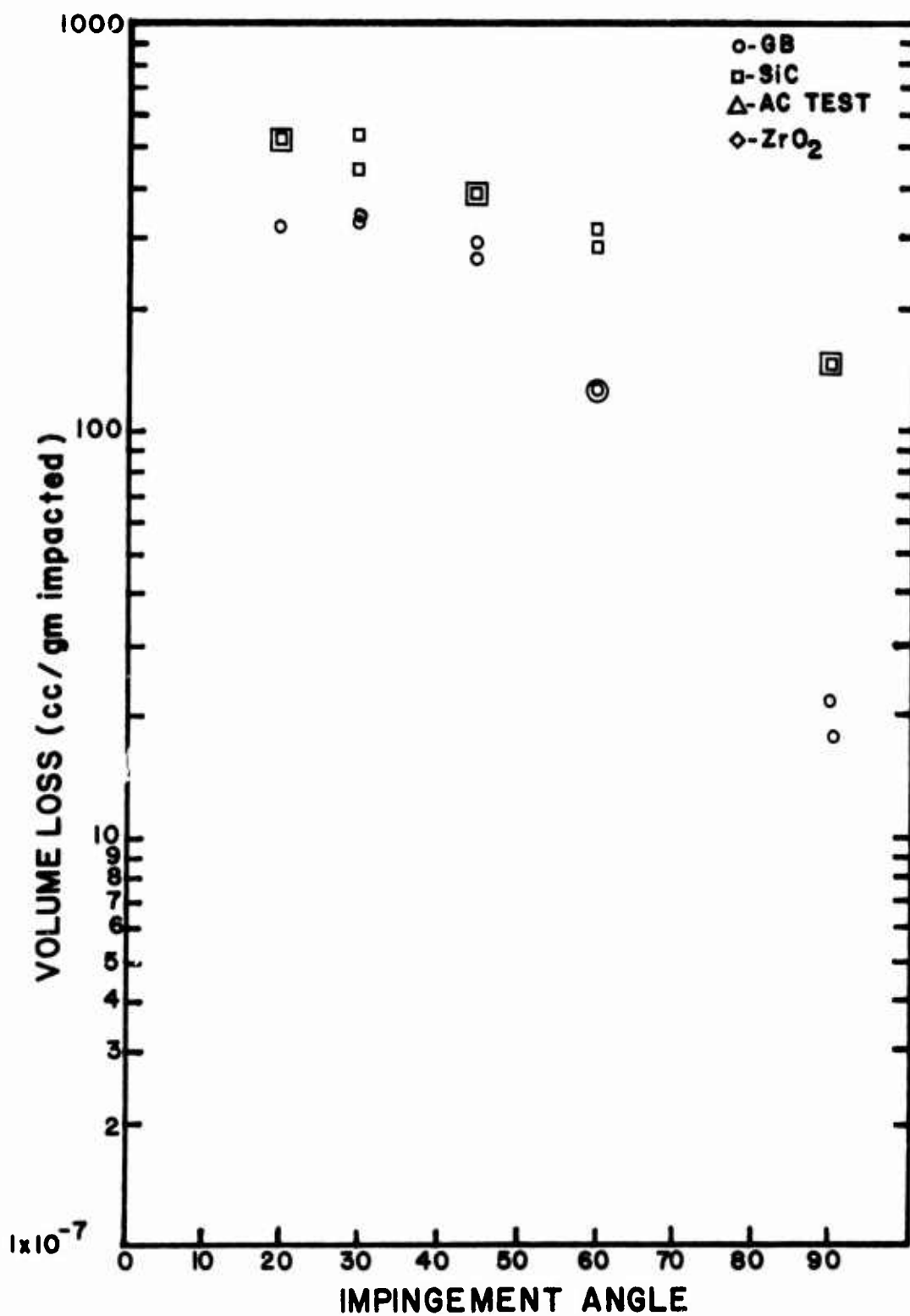


Figure 19. High Velocity Erosion of 7178 Aluminum.

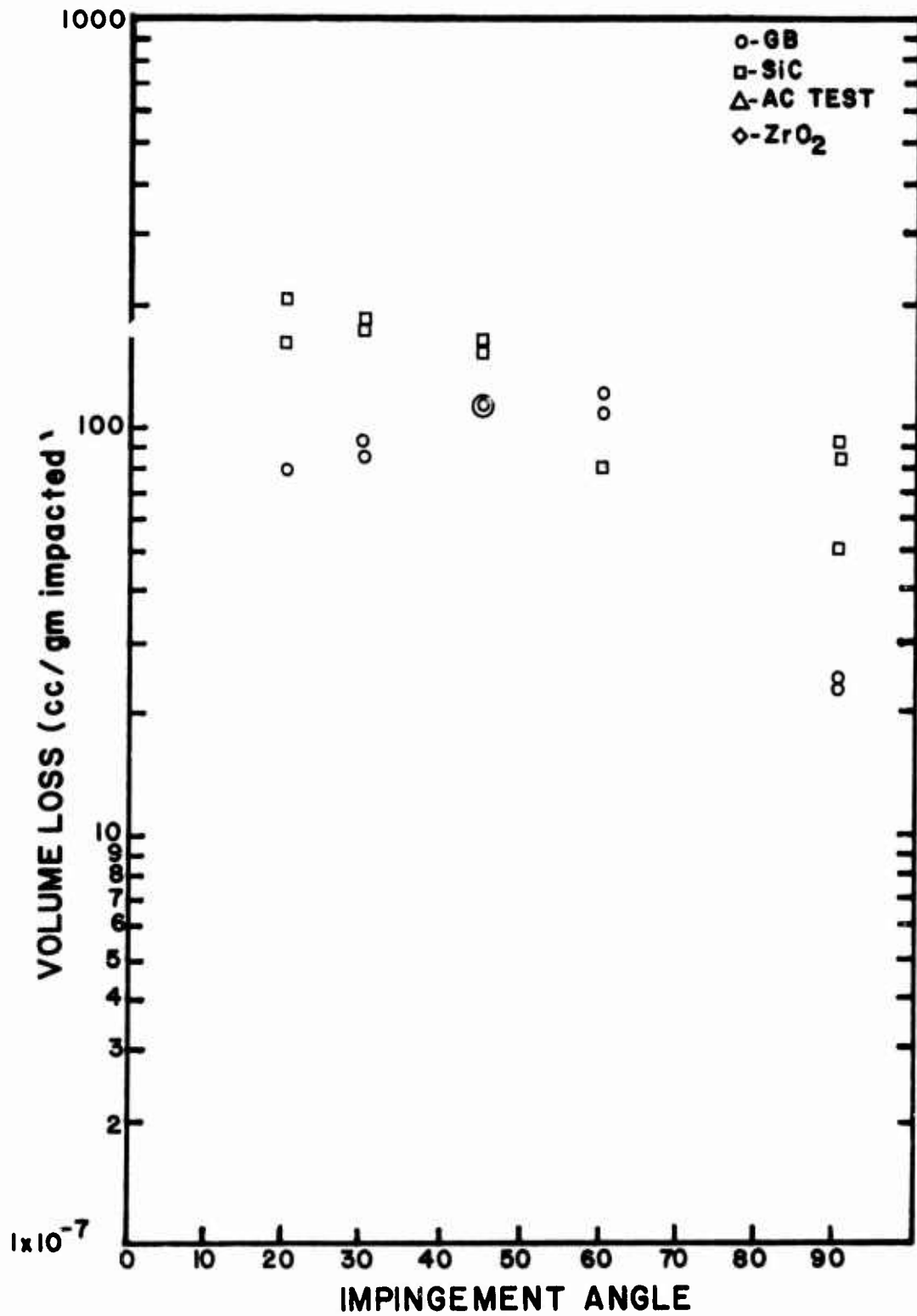


Figure 20. High Velocity Erosion of BC 25.

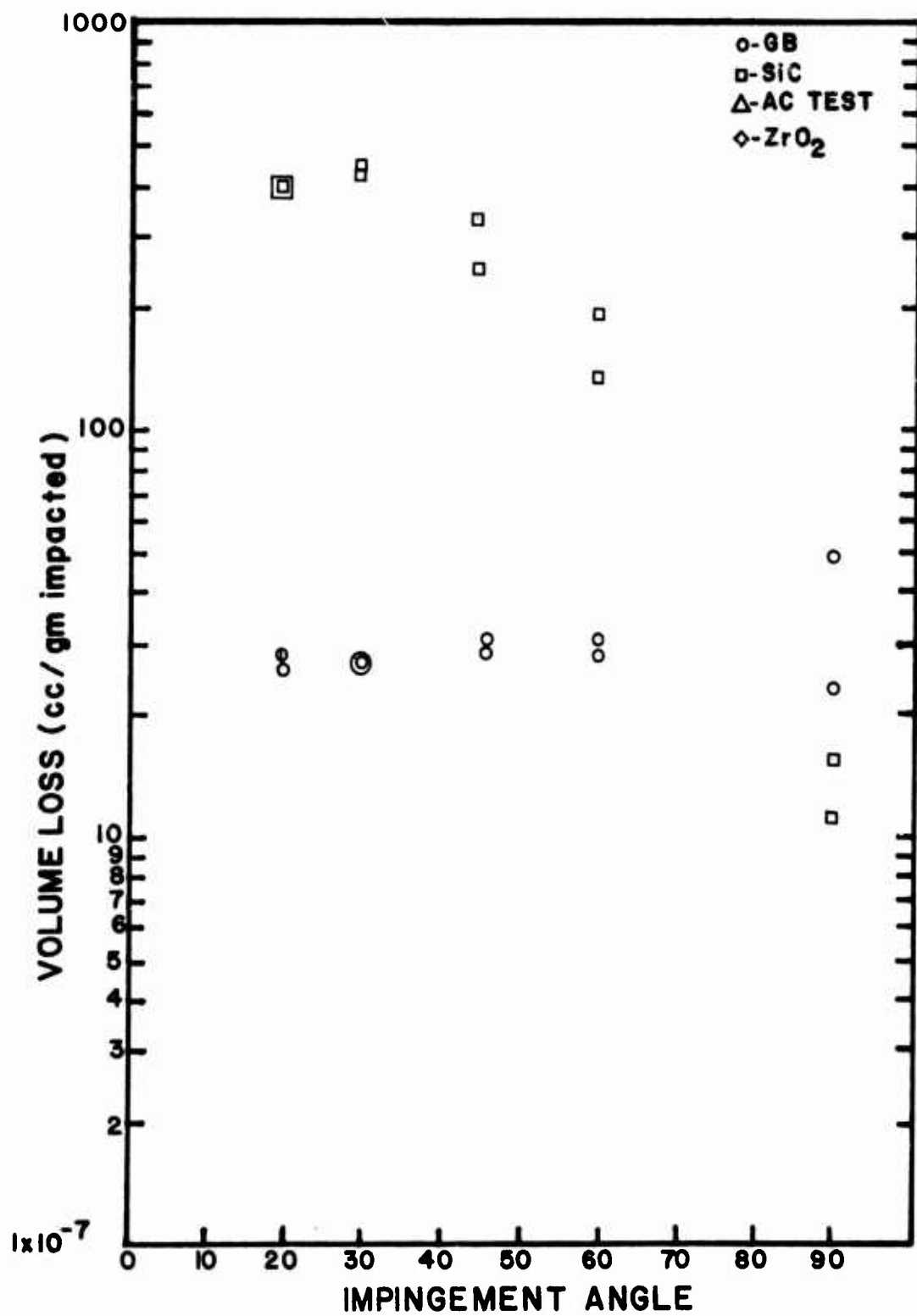
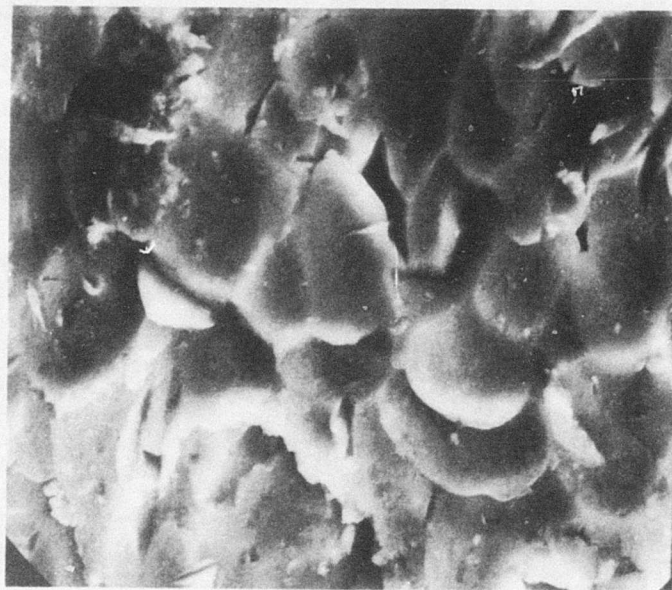


Figure 21. High Velocity Erosion of Ti 6Al-4V.



Material - 7178 Aluminum
Velocity - 91 m/sec
Impingement angle - 20°
Type of particle - Glass beads
Magnification - 1600X

Figure 22. Severely Deformed Aluminum Surface.



Material - 7178 Aluminum
Velocity - 91 m/sec
Impingement angle - 20°
Type of particle - Glass beads
Magnification - 3000X

Figure 23. Plastic Deformation of an Eroded Surface.



Material - 1100 Aluminum (Cold Worked)
Velocity - 145 m/sec
Impingement angle - 90°
Type of particle - Silicon carbide
Magnification - 450X

Figure 24. 1100 Aluminum Eroded by SiC.



Material - Ti 6-4
Velocity - 145 m/sec
Impingement angle - 90°
Type of particle - Silicon carbide
Magnification - 8000X

Figure 25. Deformed Surface of Titanium Alloy.



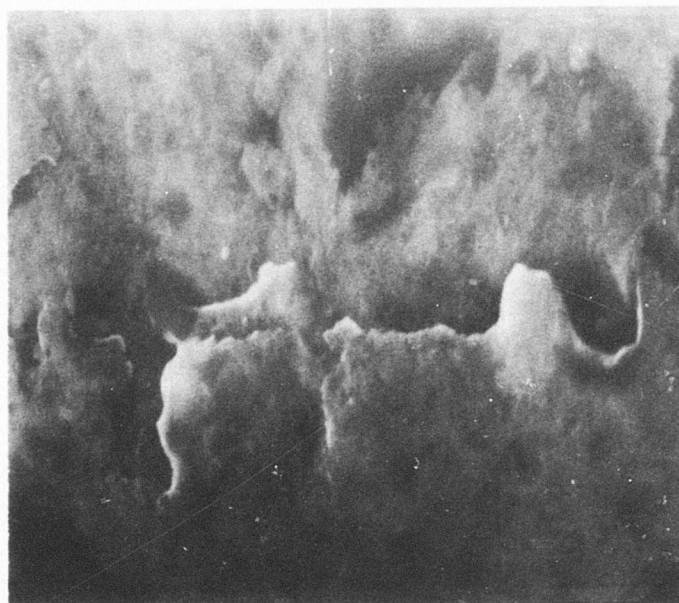
Material - 302 Stainless
Velocity - 91 m/sec
Impingement angle - 45°
Type of particle - Glass beads
Magnification - 14,000X

Figure 26. Impact Craters in 302 Stainless.

then flowed under the pressure of the gas stream or continued particle impacts. The crater shown in the center of Figure 27 contains what appears to be a once-molten droplet. This micron-sized droplet could have collected in the bottom of an impact formed crater which cooled rapidly. Even if these scanning micrographs do not show evidence of melting, such severe deformation in a period of microseconds would undoubtedly involve very large temperature effects. Therefore, it seems reasonable that the two material removal mechanisms proposed by Smeltzer et al.⁸ (splattering of molten metal upon impact and bonding of molten material to an imbedded particle and its subsequent removal) could be operating. The features noted in Figures 28 and 29 look like erosion products that were not removed during final cleaning. This debris was molten material splattered from a particle that re-bonded to the target surface upon contact. Features shown on specimen surfaces in Figures 21, 23, 24, 30, and 31 appear to be particle deposition craters. When particles were removed, some target material bonded to them was removed also.

The SEM micrographs clearly showed that target melting was the dominant erosion mechanism. However, the SEM evidence does not indicate that melting was the only material removal mechanism involved. Many SEM photographs clearly showed the presence on the eroded surfaces of a number of lips or ridges pushed up in front of impacting particles. In Figures 32-35, those ridges in samples eroded by silicon carbide closely resemble ridges produced by a bulldozer blade digging into the ground. The samples impacted by glass beads resemble a marble thrown against a mass of clay.

The ridges were not the micromachining chips theorized by Finnie. In fact, the ridges were susceptible to removal by subsequent particle impacts. A ridge formed by one particle impact and removed by a second particle impact, which in turn formed a ridge of its own, is typified in Figure 29. Ridges that have been beaten down, and when thinned, broken off, can be noted in Figures 36-39. Again, this was not the deformation wear proposed by Bitter. It appears from the SEM photographs that the erosion was neither totally a thermally activated process nor a completely mechanical one, but a combination of the two. From the work done in this investigation, it was not possible to determine just how much of the material removal process was thermally activated or how much was mechanical.



Material - Ti 6-4
Velocity - 91 m/sec
Impingement angle - 45°
Type of particle - Glass beads
Magnification - 10,000X

Figure 27. Melted Area on Titanium 6-4.



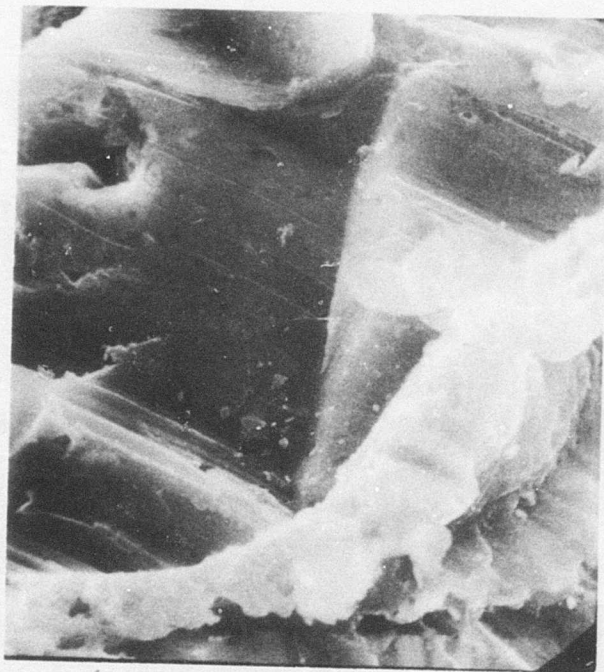
Material - 302 Stainless
Velocity - 91 m/sec
Impingement angle - 45°
Type of particle - Glass beads
Magnification - 17,000X

Figure 28. Molten Droplet in the Bottom of an Impact Crater.



Material - 7178 Aluminum
Velocity - 91 m/sec
Impingement angle - 20°
Type of particle - Glass beads
Magnification - 5500X

Figure 29. Minute Erosion Debris.



Material - 355 Aluminum
Velocity - 145 m/sec
Impingement angle - 30°
Type of particle - SiC
Magnification - 15,000X

Figure 30. Possible Splattered Droplets.



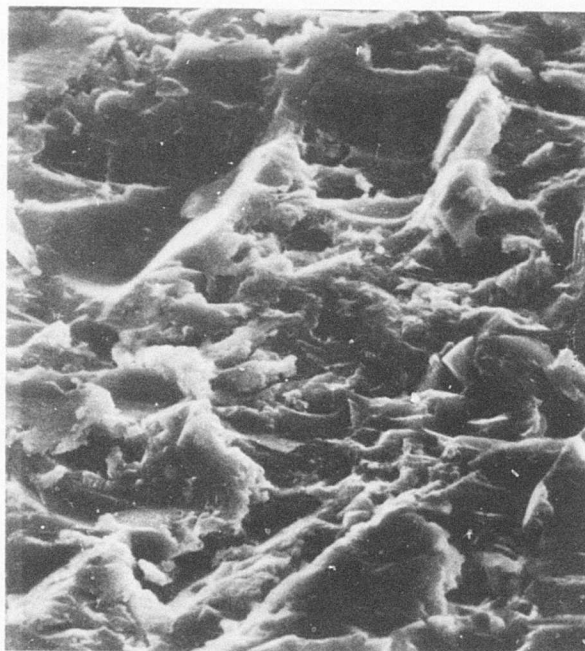
Material - 355 Aluminum
Velocity - 145 m/sec
Impingement angle - 90°
Type of particle - SiC
Magnification - 10,000X

Figure 31. Particle Deposition Craters in Aluminum Surface.



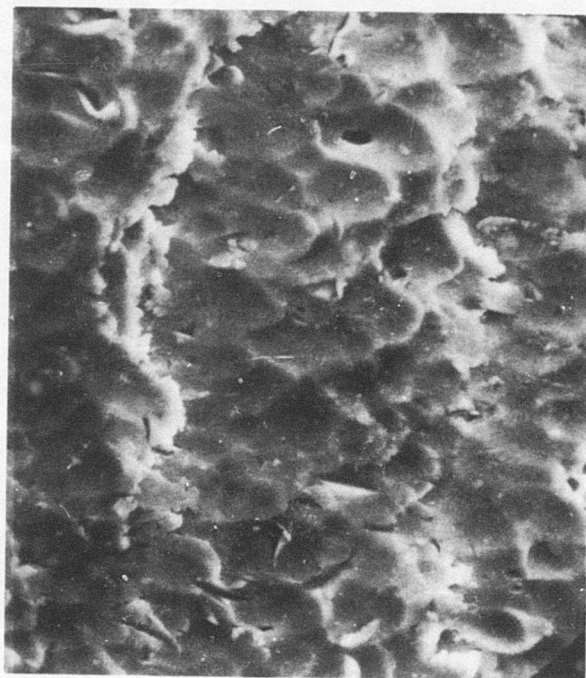
Material - 355 Aluminum
Velocity - 145 m/sec
Impingement angle - 90°
Type of particle - SiC
Magnification - 5600X

Figure 32. Surface of Aluminum Eroded by SiC.



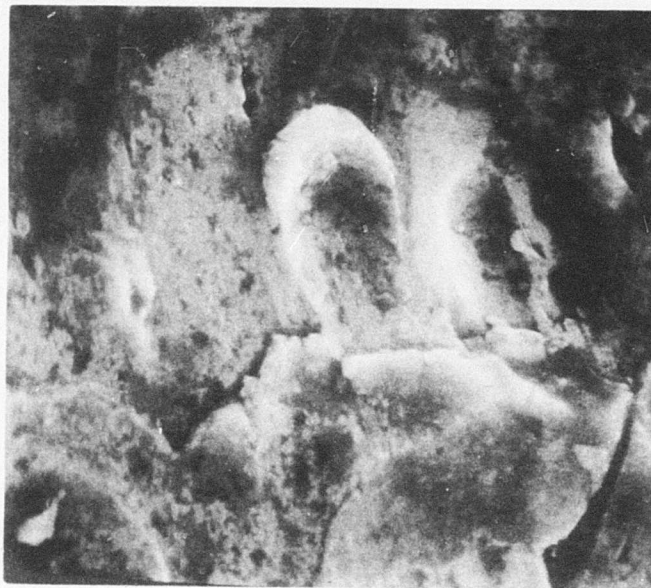
Material - 355 Aluminum
Velocity - 145 m/sec
Impingement angle - 30°
Type of particle - SiC
Magnification - 5000X

Figure 33. Ridges Pushed Up by Impacting Silicon Carbide Particles.



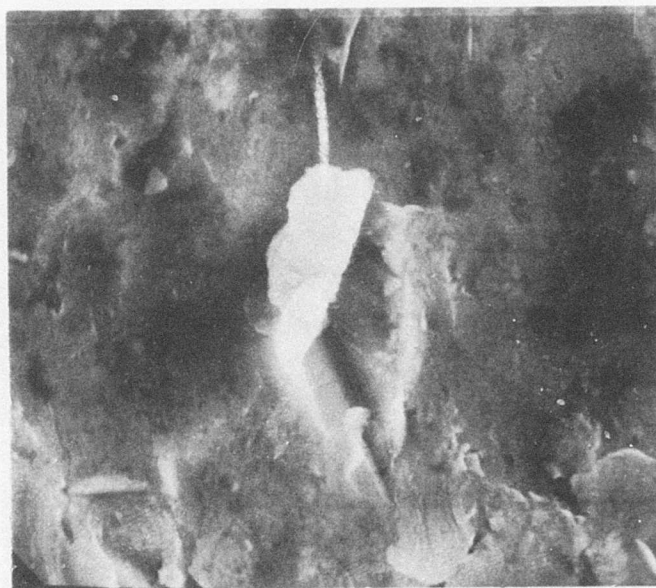
Material - 7178 Aluminum
Velocity - 91 m/sec
Impingement angle - 20°
Type of particle - Glass Beads
Magnification - 1500X

Figure 34. Ridges Produced by Impacting Glass Beads.



Material - 7178 Aluminum
Velocity - 91 m/sec
Impingement angle - 45°
Type of particle - Glass beads
Magnification - 10,000X

Figure 35. Well-Defined Ridge from a Single Glass Bead.



Material - Ti 6-4
Velocity - 145 m/sec
Impingement angle - 30°
Type of particle - SiC
Magnification - 12,000X

Figure 36. Silicon Carbide Impacting Titanium
at 30° .



Material - 355 Aluminum
Velocity - 91 m/sec
Impingement angle - 90°
Type of particle - Glass Beads
Magnification - 8000X

Figure .37. Ridge that is Flaking-Off after Further Impacts.



Material - 355 Aluminum
Velocity - 91 m/sec
Impingement angle - 90°
Type of particle - Glass Beads
Magnification - 200X

Figure 38. Severely Worked Ridges on 355 Aluminum.



Material - 355 Aluminum
Velocity - 91 m/sec
Impingement angle - 90°
Type of particle - Glass beads
Magnification - 10,000X

Figure 39. Ridges That Are About To Be Detached.

DEVELOPMENT AND VERIFICATION OF THERMODYNAMIC EROSION MODEL

MODEL DEVELOPMENT

A major objective of the research project was the development of a predictive model based on identified operative mechanisms of erosion.

Target melting was verified as a major operative mechanism of erosion during the first phase of the project. Consequently, it was felt that parameters which might appear in a predictive erosion model should reflect the resistance of materials to melting. In addition, the model should reflect the effects of the driving function, i.e., the external agent which initiated and sustained the erosion process. Finally, it was recognized that the scope of the research project was limited to nominally ductile target materials; namely, metals which were actually employed or proposed for helicopter engine applications. Therefore, it was anticipated that the model would be applicable to nominally ductile metallic materials.

The first tasks in developing a model based specifically on target melting were choosing appropriate parameters to characterize the target resistance to melting, the physical nature of the dusts, and the driving function. The following parameters were chosen on the basis of intuition, engineering judgement, and previous experience:

1. Resistance of target to melting - the density, thermal conductivity, melting temperature, enthalpy of melting, and molecular weight of the target material.
2. Physical nature of dust - the roundness of the dust.
3. Driving function - the kinetic energy transferred from the impacting particles to the target.

Erosion rate was taken as the measure of target damage.

The techniques of dimensional analysis were employed to insure that the model would be dimensionally homogeneous and to aid in assessing the form of the relationship among the variables. Details of a similar analysis are found in Reference 7.

The erosion model was as follows:

$$A = \left[\frac{(K_T)^{5/2}}{R} \frac{(G)^{1/3}}{\rho^{1/3} k T_m \Delta H_m} \right] S \quad (2)$$

where: A = target volume loss per unit mass of impacting particles
 K = kinetic energy transferred from the impacting particles to the target per unit mass of particles
 R = particle roundness
 G = gram molecular weight of target
 ρ = density of target
 k = thermal conductivity of target
 Tm = temperature of melting of target
 ΔH_m = enthalpy of melting of target
 S = dimensionless scaling factor which provides coupling between the model and the erosion test facility

For the test facility used in this investigation, the scaling factor was equal to 1.0. Because of variation in test facilities, use of other erosion data might necessitate use of an appropriate scaling factor. The model is dimensionally correct. It should be emphasized that consistent units must be associated with terms appearing in the model. In the work reported here, it was convenient to use the system of units shown in Table 4.

TABLE 4.
UNITS OF MODEL TERMS

<u>Term</u>	<u>Units</u>
A	cm^3/gm
K	$\frac{\text{gm} \cdot \text{cm}^2}{\text{gm sec}^2}$
R	No units
G	gm
ρ	gm/cm^3
k	$\frac{\text{gm} \cdot \text{cm}^2}{\text{sec}^2} \frac{\text{cm}}{\text{sec cm}^2 \text{ } ^\circ\text{K}} = \frac{\text{gm cm}}{\text{sec}^3 \text{ } ^\circ\text{K}}$
Tm	$^\circ\text{K}$
ΔH_m	$\frac{\text{gm cm}^2}{\text{sec}^2 \text{ gm}} = \frac{\text{cm}^2}{\text{sec}^2}$

Typical values* of thermal properties of the target materials are shown in Table 5.

*ASM Metals Handbook #1, 1948.

TABLE 5.
SELECTED THERMAL PROPERTIES OF TARGET MATERIALS

Matl.	Gram Molec. Wt. (gm/mole)	Density (gm/cm ³)	Thermal Conduct. (cal·cm/sec·cm ² °K)	Melting Tempera. (°K)	Enthalpy of Melting (cal/gm mole)
17-7PH	54.9	7.69	0.040	1675	65.4
17-4PH	54.9	7.81	0.043	1675	65.4
302 SS	55.6	7.90	0.039	1675	65.4
355 Al	26.9	2.71	0.360	800	94.3
7178Al	29.5	2.82	0.291	750	86.2
BC 25	63.3	8.20	0.413	1140	49.0
Ti 6-4	46.6	4.43	0.017	1923	74.4

Factors used to convert values of the typical thermal properties shown in Table 5 to the system of units used in this study (Table 4) are shown in Table 6.

TABLE 6.
CONVERSION UNITS

To obtain term	multiply listed quantities by factor F_A	F_A
G	gram molecule or weight in gm/mole	1.0
ρ	density in gm/cm ³	1.0
k	thermal conductivity in cal·cm/sec·cm ² °K	4.1868x10 ⁷
T _m	melting temperature in °K	1.0
ΔH_M	enthalpy of melting in cal/gm mole	4.1868x10 ⁷

Intuitively, the form of the erosion model is sensible. The model indicates that the erosion rate increases with increasing transferred kinetic energy. The inverse relationship between erosion rate, particle roundness, and the indicators of target resistance to melting seems reasonable. The gram molecular weight and density terms appear to assure dimensional homogeneity. The ratio of the cube roots of gram molecular weight to the cube root of the density was essentially a constant for the target materials used in this study.

MODEL VERIFICATION

Assessments of the quantities of particle kinetic energy actually transferred to targets during erosion tests were required to verify the erosion model. Representative values of particle impact and rebound velocities were obtained for combinations of particle type, impingement angle, target material type, and particle velocities (see Table 7).

TABLE 7.
COMBINATIONS OF VARIABLES EMPLOYED IN
EROSION MODEL VERIFICATION

Test Dust	Target Matls.		Impingement Angles				Max. Particle Vel.	
	Al	Ti6-4	20°	30°	45°	60°	High	Low
	X		X	X	X	X		X
Glass Beads		X	X	X	X		X	
					X		X	
	X		X		X	X		X
Silicon Carbide		X			X			X
		X	X	X	X		X	

It was recognized that both particle impact and rebound velocities were not uniform during any single test. Rather, the particle velocities were probably distributed in a manner similar to the distribution of the carrier gas velocities shown in Figure 6. It was felt that the scope and time frame of research effort effectively precluded the determination of the actual particle velocity distributions. In addition, it was believed that the actual velocity distributions were not required to verify the erosion model. As noted previously, double exposed photographs showing both impacting and rebounding particles were analyzed to determine particle velocities. Generally, numerous images of particles were visible in each photograph. The technique employed in this study consisted of determining the velocities of as many particles as possible from each photograph and discarding the high and low velocities which were typically exhibited by only a few of the particles. The impact and rebound velocities of the majority of the particles were then used in estimating the kinetic energy transferred per unit mass of impacting particles to the target by using

$$KE_T = \frac{1/2 M (V_I^2 - V_R^2)}{M} \quad (3)$$

where: V_I = impact velocity
 V_R = rebound velocity

Determinations of actual particle velocity distributions is a tedious and time-consuming task. The approach adopted in this study facilitated the acquisition of sufficient data to verify the proposed model within the time available to complete the project. A disadvantage of the approach was that erosion data generated in another research program (Reference 7) could not be used directly to verify the model developed in this study.

Verification of the thermodynamically based erosion model was attempted after estimates of transferred energy were made and particle

roundness values were established. The thermodynamic characteristics of the targets, as well as values of gram molecular weights and densities, were obtained from standard reference sources. The model was rearranged in the following form:

$$Z_T = (K_T)^{5/2} Y \quad (4)$$

where:
$$Y = \frac{G^{1/3}}{R \rho^{1/3} K T_m \Delta H_m}$$

Symbols are as defined in equation (2).

Ordered pairs of numbers were developed, viz: (A_i, Z_i) where A_i was an observed erosion rate corresponding to a target-dust combination characterized by the appropriate Y parameter and kinetic energy transfer. Points with coordinates (A_i, Z_i) were plotted on logarithmic coordinate paper, and a straight line was fitted to the points visually. The plot is shown in Figure 40.

A measure of the usefulness of the model in predicting erosion rate is the vertical deviation of the points from the line. Deviations are present, but it was felt that the model did represent the observed erosion rates very well, particularly in view of the relative dispersion of data typically obtained in erosion testing. It was concluded that the proposed erosion model was useful in estimating erosion rates and that the model could be used by others for ranking metals with respect to anticipated erosion behavior.

An attempt was made to use the model for predicting erosion rates when only particle impact velocity was employed as a measure of kinetic energy transfer. Ordered pairs of numbers were developed (A_i, Z_{iI}) where A_i represents an observed erosion rate as before but Z_{iI} has the following form:

$$Z_{iI} = (K_I)^{5/2} Y \quad (5)$$

where: Z_{iI} = erosion rate predicted on basis of kinetic energy transfer K_I

K_I = kinetic energy transferred when particle rebound velocity is zero

Y = particle and thermodynamic characterization as defined in equation (4)

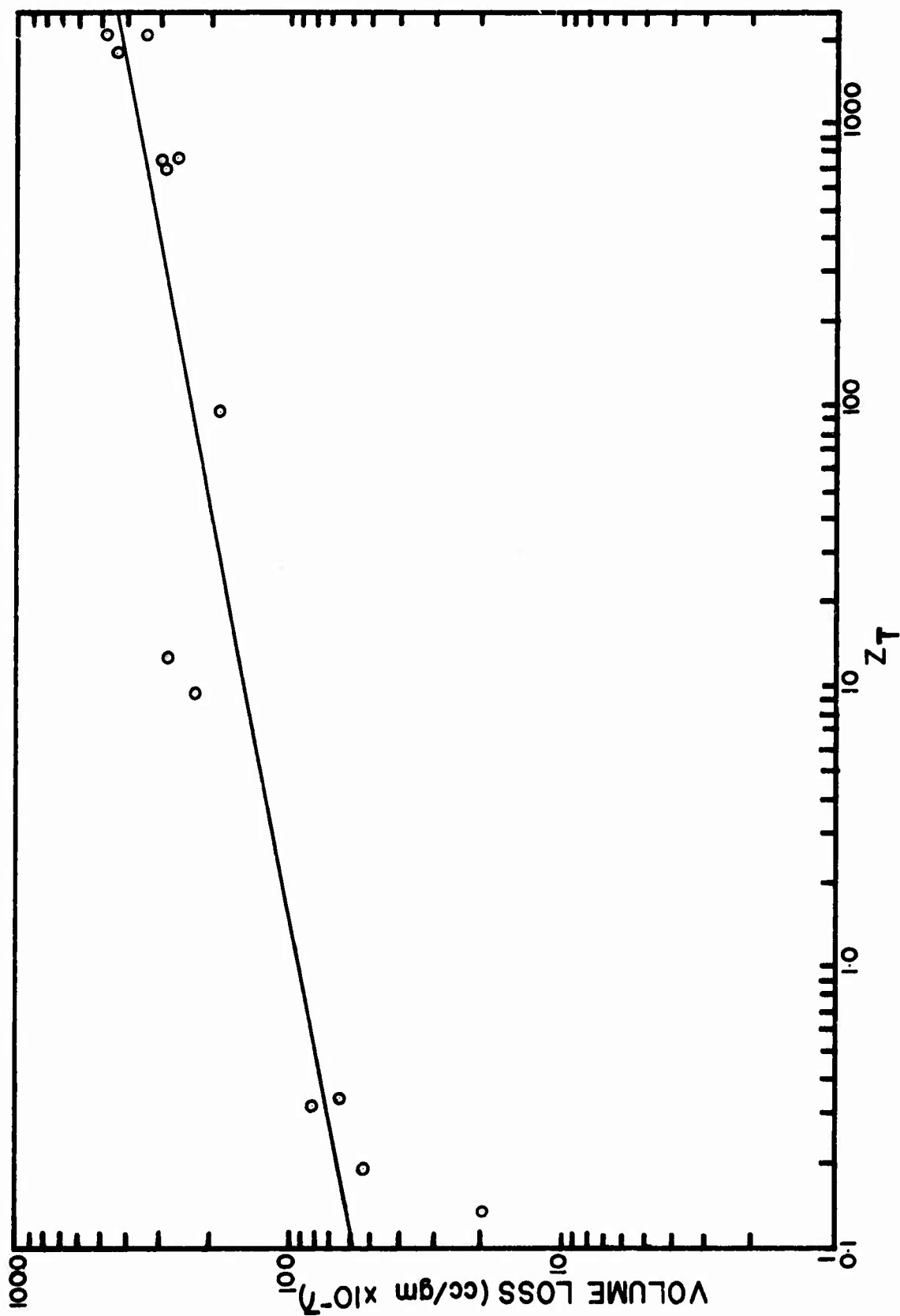


Figure 40. Line Fit of Erosion vs. $Z_{\text{Transferred}}$.

Points whose coordinates were (A_i, Z_{iI}) are plotted in Figure 41. The dispersion of the points, as anticipated, was large. An attempt to interpret the plot was abandoned.

Finally, an attempt was made to verify the model with data from an earlier study. Certain data on transferred kinetic energy were available in Reference 7 along with observed erosion rates of target materials similar to those used in this study. Data from Reference 7 were examined in the (A_i, Z_i) form; a relationship between A and Z was noted which was similar to that shown in Figure 40. The erosion rates reported in Reference 7 were higher than the erosion rates observed in this study for similar target materials. The acceleration tube of the erosion device used in the earlier work was much shorter than the tube used in the present study. The velocities of particles passing through the short tube were nearly uniform and closer to the maximum particle velocity than in the longer tube. Consequently, for similar maximum particle velocities, the energy transferred per unit of impacting particles was greater in the short tube facility than in the long tube erosion device employed in this study. Nevertheless, the additional data served as further verification of the proposed model.

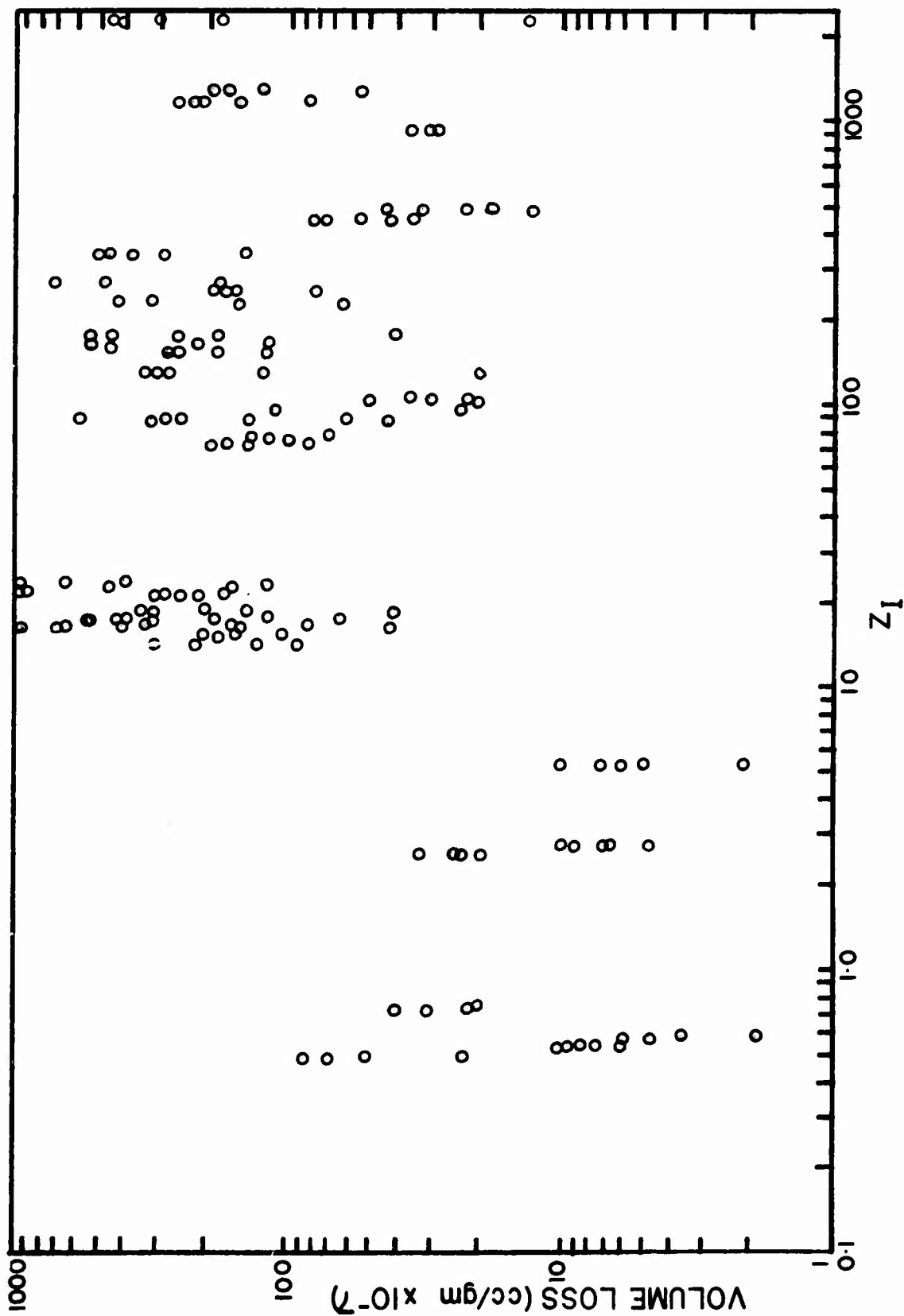


Figure 41. Erosion vs. Z_{Impact} .

CONCLUSIONS

The following conclusions appear warranted from the results of this investigation:

1. Target melting is an operative mechanism in the dust erosion of nominally ductile materials.
2. Mechanical mechanisms are also operative in the erosion process.
3. The relative contributions of each class of mechanism (thermal and mechanical) to the total damage experienced by the target are unknown at this time.
4. Mathematical models based on target melting and kinetic energy transfer can be developed for predicting ductile target erosion.
5. After certain levels of kinetic energy input have been reached, neither increasing maximum particle impact velocity nor increasing particle angularity (sharpness) have appreciable effect on the erosion rates of ductile materials.

REFERENCES

1. "The Military Significance of the Dust Problem", Proceedings of the Dust Technology Seminar, 1966, General Motors, Paper 4.
2. Finnie, I., "Erosion of Surfaces by Solid Particles", Wear, V3 (1960).
3. Bitter, J. G. A., "A Study of Erosion Phenomena: Part I", Wear, V6 (1963).
4. Bitter, J. G. A., "A Study of Erosion Phenomena: Part II", Wear, V6 (1963).
5. Neilson, J. H., and Gilchrist, A., "Erosion by a Stream of Solid Particles", Wear, V11 (1968).
6. Tilly, G. P., "A Two Stage Mechanism of Ductile Erosion", Wear, V23 (1973).
7. Head, W. J., and Harr, M. E. "The Development of A Model to Predict the Erosion of Materials by Natural Contaminants", Wear, V15 (1970).
8. Smeltzer, C. E., Gulden, M. E., McElmury, S. S., and Compton, W. A., Mechanisms of Sand and Dust Erosion in Gas Turbine Engines, USAAVLABS Tech. Report 70-36, (August 1970, AD 876584) U. S. Army Air Mobility Research and Development Laboratory, Eustis Directorate, Fort Eustis, Virginia.
9. Finnie, I., "Some Observations on the Erosion of Ductile Metals", Wear, V19 (1972).
10. Neilson, J. H., and Gilchrist, A., "An Experimental Investigation into Aspects of Erosion in Rocket Motor Tail "uzzles", Wear, V11 (1968).
11. Wood, C. D., Erosion of Metals by the High Speed Impact of Dust Particles, Proceedings of the Institute of Environmental Sciences, 1966.

DEPARTMENT OF THE ARMY

US Army Air Mobility Research and

Development Laboratory

Eustis Directorate

Fort Eustis, Virginia 23604

OFFICIAL BUSINESS

PENALTY FOR PRIVATE USE, \$300

POSTAGE AND FEES PAID
DEPARTMENT OF THE ARMY
DOD-314

